Article

SOURCE DATA | TRANSPARENT PROCESS | OPEN ACCESS

THE EMBO JOURNAL

Miro proteins prime mitochondria for Parkin translocation and mitophagy

Dzhamilja Safiulina[*,†], Malle Kuum[†], Vinay Choubey[†], Nana Gogichaishvili, Joanna Liiv, Miriam A Hickey, Michal Cagalinec[‡], Merle Mandel, Akbar Zeb, Mailis Liiv & Allen Kaasik[**]

Abstract

The Parkinson's disease-associated protein kinase PINK1 and ubiquitin ligase Parkin coordinate the ubiquitination of mitochondrial proteins, which marks mitochondria for degradation. Miro1, an atypical GTPase involved in mitochondrial trafficking, is one of the substrates tagged by Parkin after mitochondrial damage. Here, we demonstrate that a small pool of Parkin interacts with Miro1 before mitochondrial damage occurs. This interaction does not require PINK1, does not involve ubiquitination of Miro1 and also does not disturb Miro1 function. However, following mitochondrial damage and PINK1 accumulation, this initial pool of Parkin becomes activated, leading to the ubiquitination and degradation of Miro1. Knockdown of Miro proteins reduces Parkin translocation to mitochondria and suppresses mitophagic removal of mitochondria. Moreover, we demonstrate that Miro1 EF-hand domains control Miro1's ubiquitination and Parkin recruitment to damaged mitochondria, and they protect neurons from glutamate-induced mitophagy. Together, our results suggest that Miro1 functions as a calcium-sensitive docking site for Parkin on mitochondria.

Keywords calcium homeostasis; miro proteins; mitophagy; neuron; Parkin
Subject Categories Autophagy & Cell Death; Membrane & Intracellular Transport
DOI 10.15252/embj.201899384 | Received 6 March 2018 | Revised 11 October 2018 | Accepted 23 October 2018 | Published online 30 November 2018
The EMBO Journal (2019) 38: e99384

Introduction

Maintenance of proper mitochondrial function to provide cellular energy and handle calcium is essential for cell physiology, especially for highly complex cells such as neurons. Dysfunctional or depolarised mitochondria are removed by mitophagy, the selective degradation of mitochondria, to prevent cellular damage. A drop in mitochondrial membrane potential is associated with accumulation of the serine/threonine kinase PINK1 on the outer mitochondrial membrane, which together with the ubiquitin ligase Parkin, governs the elimination of defective mitochondria by mitophagy. PINK1 phosphorylates ubiquitin, and phospho-ubiquitin serves as a mitophagy signal on mitochondria (Lazarou *et al*, 2015). Phospho-ubiquitin activates Parkin (Ordureau *et al*, 2014; Okatsu *et al*, 2015; Tang *et al*, 2017), which in turn ubiquitinates mitochondrial outer membrane proteins. There are a number of Parkin substrates on the mitochondrial outer membrane (Sarraf *et al*, 2013; Martinez *et al*, 2017). Ubiquitination of TOM20 serves as the signal for mitophagy, and overexpression of TOM20 promotes mitophagy by increasing the pool of substrates available for ubiquitination (Bingol *et al*, 2014). Parkin ubiquitinates VDAC1 and VDAC3 (Geisler *et al*, 2010; Sun *et al*, 2012), and silencing of VDAC1 results in significantly reduced translocation of Parkin to damaged mitochondria and prevents mitochondrial clearance (Geisler *et al*, 2010). Ubiquitination of Mfn2 prevents fusion of damaged mitochondria and likely leads to fragmentation as fission processes remain functional (Choubey *et al*, 2014). Parkin also ubiquitinates the mitochondrial outer membrane Rho GTPases Miro1/2, which are components of the adaptor complex that anchors mitochondria to motor proteins. This leads to mitochondrial arrest and may further facilitate the removal of damaged mitochondria by mitophagy (Wang *et al*, 2011). Miro proteins directly interact with PINK1 (Weihofen *et al*, 2009; Wang *et al*, 2011; Birsa *et al*, 2014), but the role of PINK1 in Miro1 degradation remains unclear. Initial findings that PINK1 phosphorylates Miro1 at serine position 156 (Wang *et al*, 2011) were not confirmed in later studies (Liu *et al*, 2012; Birsa *et al*, 2014; Kazlauskaite *et al*, 2014a). Birsa *et al* (2014) found that mitochondrial damage triggers prompt PINK1- and Parkin-dependent Miro1 ubiquitination, while Miro2 degradation had a much slower onset. Thus, Miro1 ubiquitination rather than its degradation has been suggested to be a signal for mitochondrial arrest. A number of recent studies have focused on Miro1 as a substrate in the PINK1/Parkin pathway, and some ubiquitination sites have been identified (Sarraf *et al*, 2013; Kazlauskaite *et al*, 2014a; Ordureau *et al*, 2014; Klosowiak *et al*, 2016). Multi-monoubiquitination of Miro1 (Kazlauskaite *et al*, 2014a; Klosowiak *et al*, 2016) and an atypical lysine-27-mediated ubiquitin chain (Birsa *et al*, 2014) suggest additional roles for Miro1 ubiquitination beyond degradation.

Department of Pharmacology, Institute of Biomedicine and Translational Medicine, University of Tartu, Tartu, Estonia
*Corresponding author. Tel: +372 7374353; E-mail: dzamilja.safiulina@ut.ee
**Corresponding author. Tel: +372 7374350; E-mail: allen.kaasik@ut.ee
[†]These authors contributed equally to this work
[‡]Present address: Department of Cellular Cardiology, Institute of Experimental Endocrinology, Slovak Academy of Sciences, Bratislava, Slovakia

Furthermore, Park *et al* (2017) showed recently that Miro1 enhances Parkin catalytic activity.

Miro proteins have a unique structure as they have two GTPase domains and two Ca^{2+}-binding domains—the EF-hands (Fransson *et al*, 2003; Frederick *et al*, 2004; Guo *et al*, 2005). Miro is involved in the regulation of mitochondrial movement by Ca^{2+}, a function that requires Ca^{2+} binding to the EF-hands. This binding causes the motor/adaptor complex to dissociate from microtubules and leads to the cessation of movement (Saotome *et al*, 2008; MacAskill *et al*, 2009; Wang & Schwarz, 2009). Although the role of Ca^{2+} signalling in mitochondrial function is well defined, the involvement of Ca^{2+} in mitophagy is still poorly understood (East & Campanella, 2013; Rimessi *et al*, 2013). In neurons, glutamate-induced stress, which is tightly associated with Ca^{2+} overload, causes Parkin translocation to mitochondria (Van Laar *et al*, 2015). Inhibition of Ca^{2+} entry by voltage-gated L-type Ca^{2+} channel blockers or Ca^{2+} chelation prevents mitochondrial degradation (Cherra *et al*, 2013) and decreases PINK1 expression and mitophagy (Gómez-Sánchez *et al*, 2014). Thus, cessation of mitochondrial motility in response to elevated Ca^{2+} could be involved in the initial steps of mitophagy.

We hypothesised that Miro1 is not only a substrate for PINK1/Parkin-dependent degradation but might also have additional roles in the regulation of mitophagy. Here, we demonstrate that Miro proteins can also function as a calcium-dependent docking site and safety switch for Parkin recruitment.

Results

Silencing of Miro1 and Miro2 suppresses Parkin translocation to mitochondria

We used specific shRNAs targeted against Miro1 and Miro2 isoforms, to test whether these isoforms are required for the Parkin translocation to mitochondria. These shRNAs reduced effectively Miro1 and Miro2 expression at the mRNA level (Fig EV1A) and when combined, they almost completely inhibited mitochondrial mobility in primary cortical neurons (median mitochondrial velocity in the Miro1 and Miro2 shRNA-treated group was 4.3% of control group value, $P < 0.0001$).

We tested whether Miro proteins participate in PINK1-induced Parkin translocation to mitochondria. PC6 cells were transfected with fluorescent EYFP-Parkin, scrambled shRNA, or Miro1 and/or Miro2 shRNAs with or without untagged PINK1. PINK1 induced EYFP-Parkin translocation in approximately 20–30% of scrambled shRNA-expressing cells but in a significantly smaller proportion of Miro shRNA-expressing cells (Fig 1A and B). This cannot be explained by altered PINK1 levels because the latter was not affected in the Miro shRNAs-treated groups (Fig EV1B and C).

To measure the kinetics of Parkin translocation, we designed a time-lapse experiment where we followed EYFP-Parkin translocation in response to the respiratory chain inhibitor antimycin together with the ATP synthase inhibitor oligomycin in PC6 cells transfected with scrambled or Miro shRNAs. Cells were plated in separated compartments of the same dish allowing us to visualise Parkin translocation simultaneously and to avoid dish-to-dish variation. We then estimated the spatial heterogeneity of EYFP-Parkin fluorescence (by estimating the coefficient of variation of the intensity of pixels) in individual cells at different time points, to follow the ratio of mitochondrial-to-cytosolic Parkin. Further statistical analysis of these data (39–47 cells from each group) demonstrated that Miro shRNAs reduced Parkin translocation significantly (Fig 1C) with the number of cells showing Parkin translocation being significantly lower in Miro shRNA-expressing cells (Fig 1D).

We also estimated mitophagy using the mitochondrially targeted pH-dependent protein Keima, the excitation spectrum of which shifts when mitochondria are delivered to acidic lysosomes. Similar to Parkin translocation, mitophagy was increased in PINK1-expressing PC6 cells and was suppressed when Miro shRNAs were co-expressed (Fig 1E). However, it should be noted that the overall intensity of the Keima signal was lower in Miro shRNAs-expressing PC6 cells, making the ratiometric analysis prone to artefacts. We therefore performed additional mitochondrial Keima experiments in neurons expressing both Miro shRNAs and counted the number of mitochondria in an acidic environment manually. We were not able to perform this experiment with PINK1 or antimycin with oligomycin because of their toxicity in neurons. Nevertheless, the data show an almost twofold decrease in basal mitophagy in response to Miro knockdown (Fig 1F). Miro shRNAs also led to an almost twofold decrease in the number of mitochondria co-localising with the autophagosome marker, EGFP-LC3B (Fig 1G).

We also excluded the possibility that the change in mitochondrial motility associated with Miro loss has a primary role in the change in Parkin recruitment. Figure EV2A shows that overexpression of Syntaphilin, which inhibits mitochondrial motility similar to Miro shRNAs (median mitochondrial velocity in the Syntaphilin-overexpressing group was 5.0% of control group value, Fig EV2B), neither induced Parkin translocation nor affected Parkin translocation in the presence of PINK1 or antimycin and oligomycin (A&O). This suggests that inhibition of mitochondrial movement *per se* cannot be the primary reason for the altered Parkin translocation.

Thus, these set of data allow us to conclude that Miro proteins are required for appropriate Parkin translocation and initiation of mitophagy.

Miro1 recruits Parkin to polarised mitochondria

When performing control experiments, we observed, to our surprise, that overexpression of myc-Miro1 changed Parkin localisation in the cytosol. However, the translocation pattern was completely different from PINK1- or A&O-induced Parkin translocation. In the case of PINK1 or A&O, a majority of cytosolic EYFP-Parkin translocated to a few strong individual puncta that did not cover the entire mitochondrial network (Fig 2A middle panels). In Miro1-overexpressing cells, however, the EYFP-Parkin inclusions were relatively dull and not as bright as in PINK1-overexpressing or A&O-treated cells (Fig 2A lower panels). Moreover, in Miro1-overexpressing cells, EYFP-Parkin overlapped with the mitochondrial network and did not show puncta-like structures as in A&O-treated cells.

The results depicted in Fig 2B (left panel) show that the percentage of cells in which Parkin translocated to mitochondria in Miro1-overexpressing groups was similar to PINK1 overexpression (Fig 1B) or A&O treatment (Fig 1D). However, this assay does not show the strength of Parkin translocation, i.e., the amount lost from the diffuse cytosolic pool. On the other hand, the heterogeneity assay depicted in Fig 2C does show that the strength of Parkin

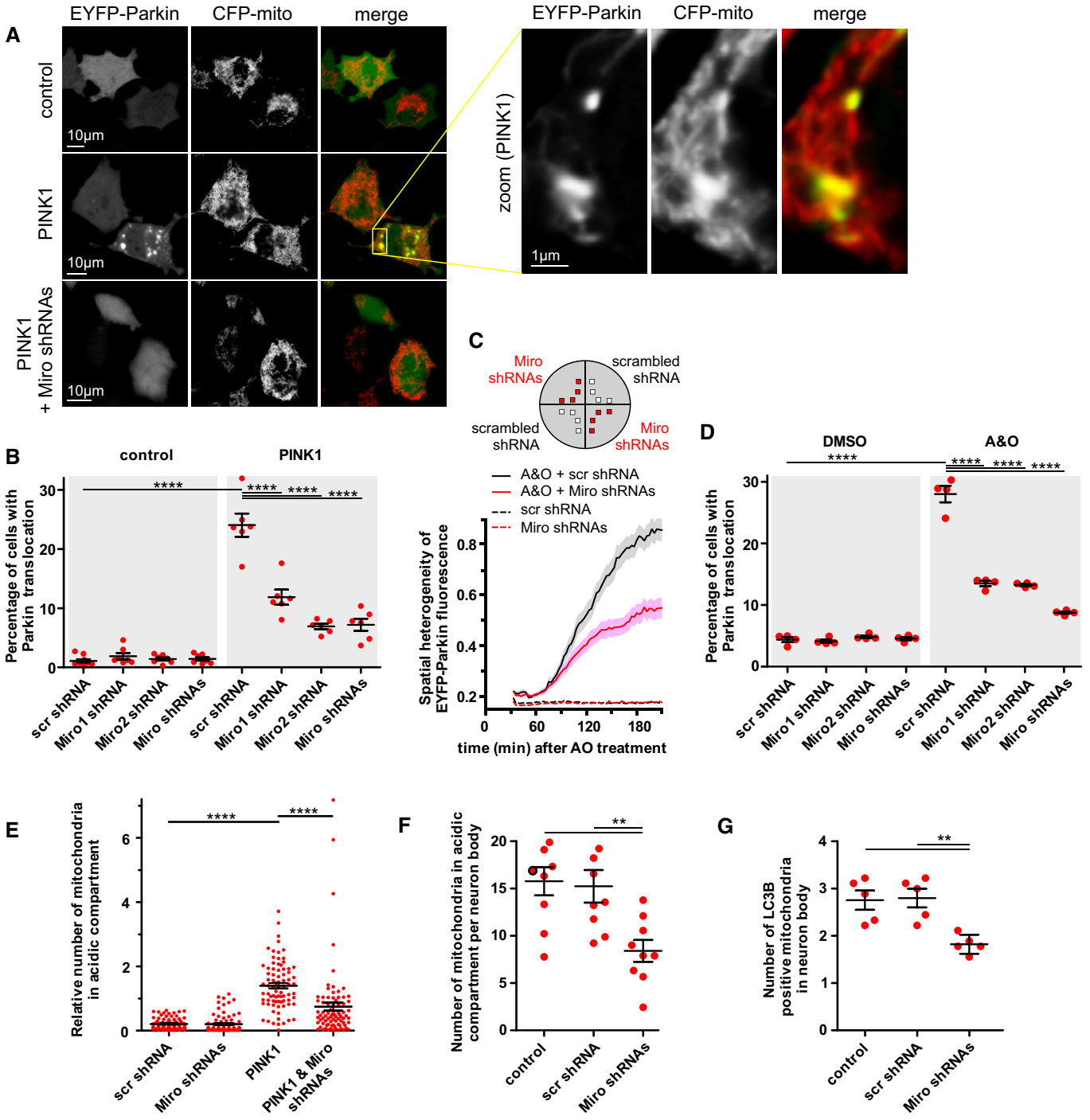

Figure 1.

translocation from cytosol to mitochondria within single Miro1-expressing cells is weaker when compared with PINK1-overexpressing or A&O-treated cells. Thus, Miro1 induces Parkin translocation in a similar proportion of cells to other treatments but the translocation in individual cells is significantly weaker.

Miro1-induced Parkin translocation was not limited to PC6 cells as Miro1 overexpression induced similar effects in MEFs and primary cortical neurons (Appendix Fig S1).

We next tested whether we could also induce Parkin translocation by overexpressing Miro2. However, overexpression of myc-Miro2 had no effect on Parkin localisation (Fig 2B, left panel) when compared with myc-Miro1 (same plasmid backbones; Fransson *et al*, 2003). This could be, however, explained by cellular mislocalisation of myc-Miro2, which remained largely cytosolic, while overexpressed myc-Miro1 was perfectly co-localised with a mitochondrial marker (Appendix Fig S2). We therefore repeated this

Figure 1. Miro1 and Miro2 are required for Parkin translocation to mitochondria and mitophagy.

A Representative pseudocolour images of PC6 cells transfected with EYFP-Parkin (green) and mitochondrially targeted CFP (red) with and without PINK1 and Miro1 shRNA and Miro2 shRNA. Zoomed images show translocation of EYFP-Parkin to mitochondria in PINK1-overexpressing PC6 cells.

B Quantification of EYFP-Parkin translocation to mitochondria. The percentage of PC6 cells with EYFP-Parkin translocated to mitochondria in response to PINK1 overexpression is lower in the Miro shRNAs-expressing groups when compared with the scrambled shRNA-expressing group (scr shRNA). ****$P < 0.0001$, $n = 6$ dishes per group, 20 fields per dish, one-way ANOVA.

C The kinetics of EYFP-Parkin translocation is different in PC6 cells transfected with scrambled or Miro shRNAs. Cells were plated in separate compartments of the same dish, enabling us to visualise Parkin translocation simultaneously over 3 h under similar conditions in response to antimycin with oligomycin treatment (A&O, both 10 μM). The spatial heterogeneity of EYFP-Parkin (coefficient of variation of the intensity of individual pixels) was estimated for individual cells for each time point ($n = 39$–47 cells; $P < 0.0001$ difference between the curves $P < 0.0001$, two-way ANOVA; lines show mean, dashed area shows SEM).

D Miro shRNAs mitigate the effect of A&O on EYFP-Parkin translocation. PC6 cells transfected with EYFP-Parkin with and without Miro shRNAs were treated with DMSO or A&O (both 10 μM) for 3 h. The figure demonstrates that the percentage of cells with Parkin translocated to mitochondria was lower in the Miro shRNAs-expressing group when compared with the scrambled shRNA-expressing group. ****$P < 0.0001$, $n = 4$ dishes, 20 fields per dish, one-way ANOVA.

E Miro shRNAs inhibit PINK1-induced mitophagy in PC6 cells. The figure shows the changes in the excitation spectra of mitochondrially targeted pH-sensitive Keima (ratio of 561 nm/458 nm fluorescence intensities). ****$P < 0.0001$, $n = 80$ cells from 4 dishes, Kruskal–Wallis test.

F Miro shRNAs inhibit basal mitophagy in primary cortical neurons expressing mitochondrially targeted Keima. Mitochondria in lysosomes (acidic pH) were counted manually, by a blinded observer (**$P < 0.01$, $n = 9$ dishes, 9 fields per dish, from two independent experiments, one-way ANOVA).

G Miro shRNAs decrease the number of mitochondria co-localised with the autophagosome marker EGFP-LC3B in primary cortical neurons (**$P < 0.01$, $n = 5$ dishes, 9 fields per dish, one-way ANOVA).

Data information: Data are presented as means ± SEM.
Source data are available online for this figure.

experiment using untagged Miro2 that localised clearly to mitochondria and induced strong Parkin translocation (Fig 2B, right panel). These results suggest that Miro1 and Miro2 act redundantly in this case.

Miro1 overexpression did not induce mitochondrial depolarisation but instead led to slight hyperpolarisation (Fig 2D and E) consistent with a previous report in *Drosophila* (Babic *et al*, 2015). Notably, Miro1 overexpression-induced Parkin translocation did not induce significant degradation of Miro1 in HEK cells at control conditions but only when the cells were treated with A&O (Fig 2G). Also, co-expression of Parkin and Miro1 did not inhibit mitochondrial trafficking (Fig 2F, Appendix Fig S3), as we initially expected (as previously reported by Wang *et al*, 2011), suggesting that Miro has remained functional.

These microscopy findings were supported by co-immunoprecipitation experiments. Figure 2H shows that Parkin co-immunoprecipitates with Miro1 under basal conditions, i.e., without applying mitochondrial uncouplers or inhibitors of the respiratory chain. This interaction became stronger when cells were treated with A&O. In the latter case, we noted a number of higher molecular weight bands positioned approximately 9 and 20 kDa above Miro1, suggesting Miro1 (poly)ubiquitination. Furthermore, we show that the Miro1-Parkin interaction can be detected between

Figure 2. Miro1 recruits Parkin to polarised mitochondria.

A The pattern of Parkin translocation caused by Miro1 overexpression is different from A&O-induced translocation. The figure illustrates puncta-like EYFP-Parkin on mitochondria in antimycin and oligomycin-treated (both 10 μM for 3 h) PC6 cells (middle panels), whereas in Miro1-overexpressing cells, EYFP-Parkin appears along rod-shaped mitochondria visualised with CFP-mito (lower panels). The merged panels present EYFP-Parkin (green) and CFP-mito (red).

B Overexpression of myc-Miro1 and untagged Miro2, but not myc-Miro2, induced EYFP-Parkin translocation to mitochondria. ****$P < 0.0001$ versus control group, $n = 5$–6 dishes, 20 fields per dish, one-way ANOVA or *t*-test.

C Quantification of EYFP-Parkin signal heterogeneity in PC6 cells demonstrates that Miro1 overexpression induces Parkin translocation from the cytosol to mitochondria, which is significantly weaker than PINK1 overexpression- or A&O (3 h)-induced translocation. **$P < 0.01$ and ****$P < 0.0001$ versus control group, $n = 18$–32 cells from 3 dishes per group, Kruskal–Wallis test.

D, E Miro1 overexpression does not cause mitochondrial depolarisation. (D) Representative image of Miro1 and EYFP-Parkin-transfected cells stained with TMRE. The merged panels present EYFP-Parkin (green) and TMRE (red). (E) Relative TMRE intensity quantified in neurons transfected with Miro1 (detected by CFP-mito co-transfection); the control group is non-transfected cells in the same image. The relative TMRE signal was slightly increased in Miro1 overexpressing neurons but unaffected in Miro shRNAs-expressing neurons. Note that FCCP treatment (3 μM for 15 min) almost completely abolished TMRE fluorescence. ****$P < 0.0001$ versus control group, $n = 94$–186 cells from 4 dishes per group, Kruskal–Wallis test.

F Co-expression of HA-Parkin with Miro1 does not suppress mitochondrial motility in axons of cortical neurons. Overexpression of Miro1 alone increased the motion time in both directions as well as the relative mitochondrial velocity. Co-transfection of Parkin did not affect significantly the motility parameters. Data are presented as Tukey boxplot. *$P < 0.05$, **$P < 0.01$, ***$P < 0.001$ and ****$P < 0.0001$, $n = 689$–846 individual mitochondria from 39 to 44 axons per group pooled from at least from 10 individual dishes from 4 independent experiments, Kruskal–Wallis test.

G Parkin overexpression does not induce degradation of myc-Miro1 in control conditions. Representative Western blot image and analysis of myc-Miro1 expression in HEK cells. Treatment with A&O (both 15 μM) for 3 h in the absence of MG132 led to slight degradation of myc-Miro1. Co-expression of EYFP-Parkin did not induce degradation of Miro1 although an additional band above the Miro1 band was present. However, Parkin co-expression enhanced Miro1 degradation when cells were treated with A&O. *$P < 0.05$ and ****$P < 0.0001$, ns: not significant, $n = 4$ independent experiments, one-way ANOVA. Note that only the main band of myc-Miro1 at 80 kDa was analysed and that YFP was used to compensate in groups not expressing EYFP-Parkin.

H EYFP-Parkin co-immunoprecipitates with overexpressed myc-Miro1, both in DMSO- and in A&O (both 15 μM for 3 h)-treated HEK cells.

I Endogenous Parkin co-immunoprecipitates with endogenous Miro1. Miro1 was immunoprecipitated from non-transfected and non-treated HEK cells using mouse monoclonal anti-Miro1 antibody and immunoblotted for endogenous Parkin.

Data information: Data are presented as means ± SEM or as a Tukey plot (median ± 1.5 times interquartile range).
Source data are available online for this figure.

endogenous proteins (Fig 2I). Note that we also observed interaction between overexpressed untagged Miro2 and Parkin (Appendix Fig S4).

Thus, these data suggest that Miro1 is able to attract cytosolic Parkin to mitochondria without affecting the mitochondrial membrane potential or its own degradation.

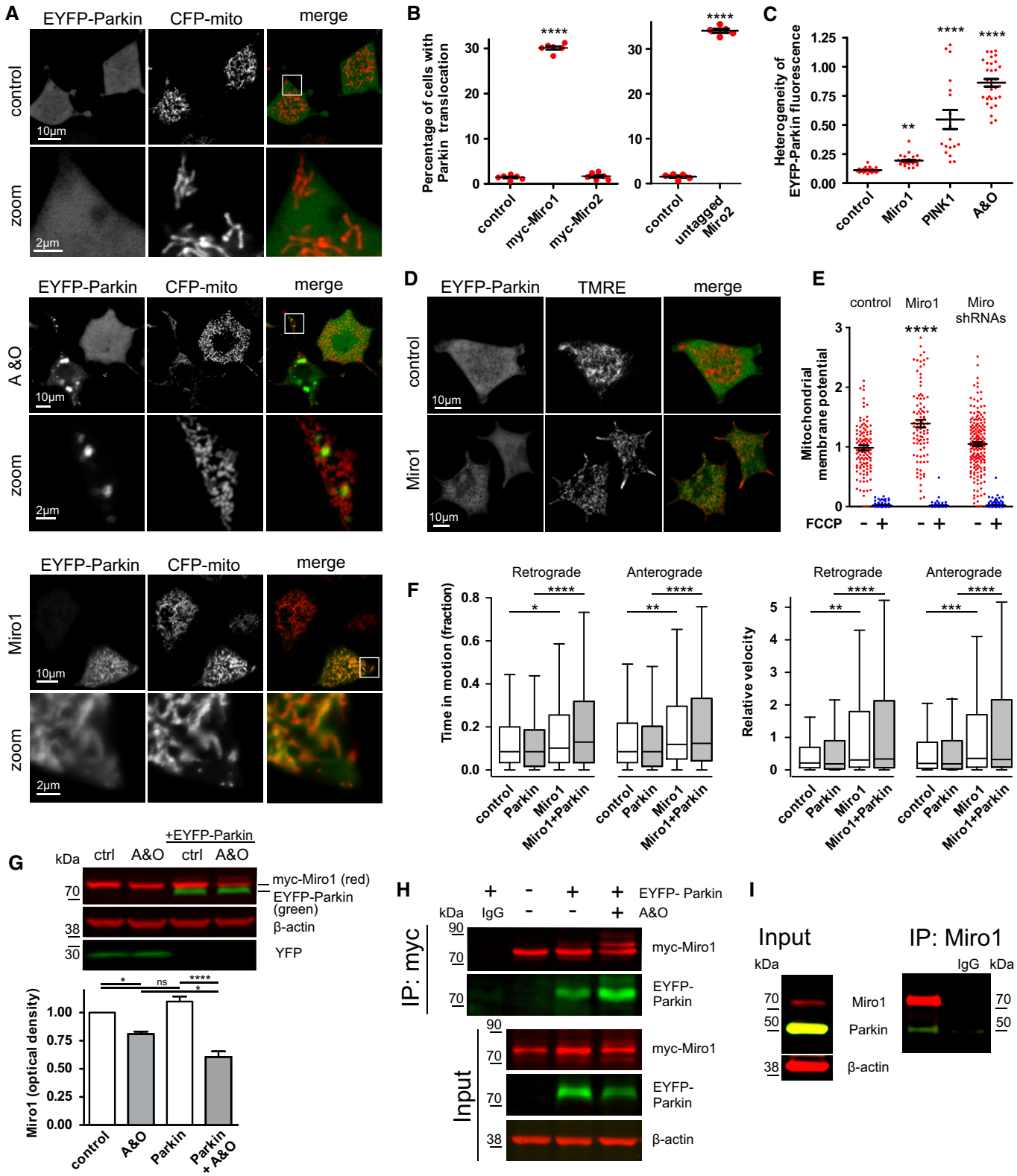

Figure 2.

Miro1 recruits Parkin independently of PINK1 and of Parkin E3 ubiquitin ligase activity

To test whether PINK1 is required for Miro1-induced Parkin translocation to mitochondria, we first suppressed endogenous PINK1 using specific shRNA (Choubey *et al*, 2014). Miro1 overexpression also induced Parkin translocation in PC6 cells transfected with PINK1 shRNA, whereas no Parkin translocation was observed when PINK1 shRNA-expressing cells were treated with the A&O (Fig 3A; note that the graphs depict the percentage of cells showing translocation not the strength of translocation itself: Miro1-induced Parkin translocation was relatively weak whereas in A&O-treated groups it was very strong). To exclude the possibility that the low remaining level of PINK1 after shRNA silencing was sufficient for Miro1-induced Parkin translocation, we repeated a similar experiment in MEFs prepared from PINK1-deficient mice. Miro1 overexpression led to Parkin translocation in PINK1-deficient MEFs (Fig 3B), but A&O failed to induce any significant Parkin translocation in PINK1-deficient MEFs. Interestingly, we observed that overexpressed Miro1 intensities were slightly higher in PINK1$^{-/-}$ MEFs (Appendix Fig S5) suggesting that a lack of PINK1 may inhibit Miro1 ubiquitination and subsequent removal.

We next tested whether Miro1-induced Parkin translocation required the E3 ligase activity of Parkin. We overexpressed the ligase-dead Parkin mutant T240R (associated with autosomal recessive juvenile parkinsonism, Hattori *et al*, 1998) as well as C431N (which can self-associate in response to mitochondrial depolarisation but cannot translocate to mitochondria, Lazarou *et al*, 2013). However, these mutants were recruited to mitochondria as efficiently as wild-type Parkin when Miro1 was overexpressed (Fig 3C). As expected, both mutants failed to translocate to mitochondria as efficiently as WT in response to A&O treatment only (Fig 3C). We also tested whether the Parkin mutants interacted with Miro1. C431N and T240R Parkin interacted with Miro1 both in untreated and in A&O-treated cells but they were not able to induce the ladder of higher molecular weight bands of Miro1 (Fig 3D).

Altogether, this set of experiments show that Miro1 recruitment of Parkin to mitochondria is independent of PINK1 and Parkin ubiquitin ligase activity (although endogenous Parkin might have a complementary role in this setting). This also suggests that Parkin does not need to be activated in order to interact with Miro1 (its activation might occur after interaction with Miro) and that inactive Parkin mutants can interact with Miro1 and further, that Miro1 could indeed act as a docking station for autoinhibited Parkin.

Parkin recruitment to mitochondria is two-step process

Data from *in vitro* ubiquitination assays suggest that Parkin preferentially targets lysine K572 in the Miro1 C-terminal GTPase (Kazlauskaite *et al*, 2014a; Klosowiak *et al*, 2016). We asked therefore whether mutation of this lysine to arginine, which prevents Miro1 ubiquitination at this site, affects Parkin recruitment to mitochondria. We first tested whether Parkin could interact with and ubiquitinate Miro1 K572R. Co-immunoprecipitation experiments revealed that K572R mutation does not abolish the interaction between myc-Miro1 and HA-Parkin (Fig 4A). We then co-expressed WT or K572R Miro1 with EYFP-Parkin and ubiquitin-HA,

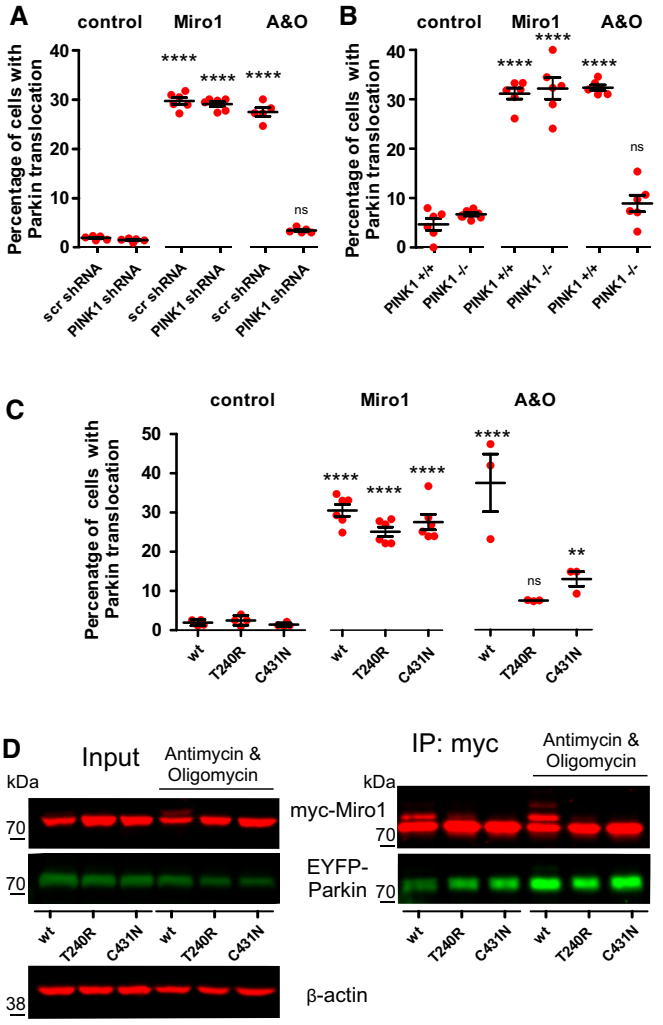

Figure 3. Miro1-induced Parkin translocation to mitochondria does not require PINK1 and is independent from E3 ligase activity of Parkin.

A Miro1 induces EYFP-Parkin translocation in the presence of PINK1 shRNA. PC6 cells were transfected with EYFP-Parkin and Miro1 or treated for 3 h with A&O (both 10 μM) in the presence of scrambled shRNA or PINK1 shRNA. Miro1 induced Parkin translocation also in the presence of PINK1 shRNA while A&O treatment did not. ****$P < 0.0001$ compared with the respective control group, n = 5–6 dishes, 20 fields per dish, one-way ANOVA.

B Miro1 induces EYFP-Parkin translocation in PINK1$^{-/-}$ MEFs. MEFs obtained from PINK1$^{+/+}$ and $^{-/-}$ mice were transfected with EYFP-Parkin and Miro1 or treated with A&O (both 10 μM for 3 h). Miro1 induced Parkin translocation in both MEF lines but A&O only in PINK1$^{+/+}$ MEFs. ****$P < 0.0001$ compared with respective control group, n = 6 dishes, one-way ANOVA.

C Mutated EYFP-Parkin is recruited to mitochondria in response to Miro1 overexpression. PC6 cells were transfected with wild type, T240R or C431N EYFP-Parkin and Miro1 or treated for 3 h with A&O (both 10 μM). Miro1 induced translocation of all EYFP-Parkin mutants whereas A&O treatment was not able to induce equivalent translocation of Parkin mutants. **$P < 0.01$ and ****$P < 0.0001$ compared with respective control group, n = 3–6 dishes, 20 fields per dish, one-way ANOVA.

D Parkin mutants T240R and C431N interact with Miro1 both in DMSO- or A&O-treated (both 15 μM for 3 h) HEK cells. Note that the higher molecular weight bands of Miro1 were observed only in WT Parkin-expressing groups.

Data information: Data are presented as means ± SEM.
Source data are available online for this figure.

immunoprecipitated the ubiquitin-HA and probed for Miro1. As expected, we observed reduced ubiquitination of the K572R Miro1 mutant (Fig 4B), indicating that efficient Miro1 ubiquitination occurs only when K572 is intact. Note that Miro K572R was also more resistant to A&O-induced degradation (42 ± 2% Miro1 WT versus 62 ± 10% Miro1 K572R left after 3-h treatment; $P = 0.03$, $n = 4$, Mann–Whitney test).

We next tested whether Miro1 K572R could affect Parkin translocation to mitochondria. As depicted in Fig 4C (upper panel), overexpression of Miro1 K572R induced Parkin translocation to rod-shaped structures identical to Miro1 WT-induced Parkin translocation. Thus, initial recruitment of Parkin by Miro1 does not involve ubiquitination of Miro1 at K572.

However, we wondered whether the K572R might affect A&O-induced Parkin translocation. We therefore designed an experiment allowing us to separate between the weak and strong Parkin translocation using spatial heterogeneity analysis of EYFP-Parkin translocation at baseline and subsequent to A&O. The results shown in Fig 4D demonstrate that both Miro1 WT and Miro1 K572R induced similar initial (weak) Parkin translocation but only the WT form potentiated A&O-induced Parkin translocation. Note that Miro1 K572R was otherwise fully functional as it was able to restore mitochondrial motility in Miro shRNAs-expressing neurons to a level similar to Miro1 WT (Fig EV3). Furthermore, Ca^{2+}-induced arrest of mitochondrial motility in Miro1 K572R-overexpressing neurons was similar to WT Miro1 (Fig EV3C).

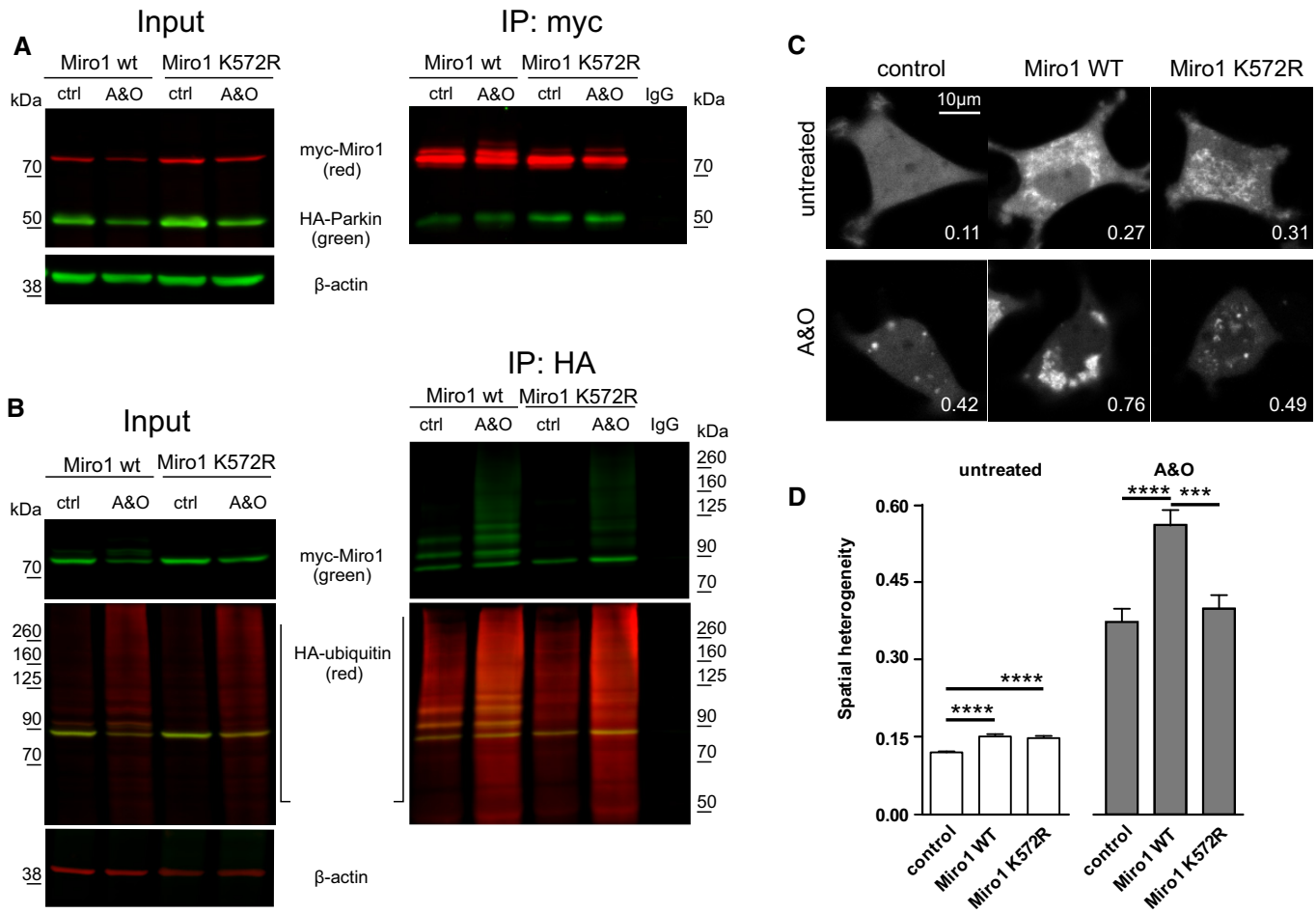

Figure 4. Prevention of Miro1 ubiquitination at K572 reveals two steps in Parkin recruitment to mitochondria.

A Miro1 K572R mutant interacts with HA-Parkin similarly to Miro1 WT. HEK cells overexpressing myc-Miro1 WT or K572R mutant were treated with DMSO (control) or A&O (both 15 μM) for 3 h. Myc-Miro1 was immunoprecipitated and probed for myc-Miro1 and HA-Parkin. Note the diminished degradation of Miro1 K572R in input and the additional band above Miro1 WT in the IP, which is missing in the case of the K572R mutant.

B Miro1 K572R ubiquitination by Parkin is reduced. HEK cells overexpressing HA-ubiquitin, myc-Miro1 or myc-Miro1 K572R and EYFP-Parkin were treated with DMSO (control) or A&O (both 15 μM) for 3 h. HA-ubiquitin was immunoprecipitated and probes were immunoblotted for ubiquitin-HA and myc-Miro1.

C Representative images of PC6 cells overexpressing Miro1 K572R or Miro1 WT together with EYFP-Parkin. K572R mutant induces Parkin translocation similar to WT in basal conditions but not after treatment with A&O (both 7.5 μM) for 3 h. Note the spatial heterogeneity values shown in the images.

D Quantification of EYFP-Parkin signal heterogeneity in PC6 cells demonstrates that WT Miro1 overexpression amplifies Parkin translocation in response to A&O (both 7.5 μM) treatment for 3 h, but K572R mutation of Miro1 abolishes this effect. ***$P < 0.001$ and ****$P < 0.0001$, n = 152–172 cells from 3 dishes per group, Kruskal–Wallis test. Data are presented as means ± SEM.

Source data are available online for this figure.

These experiments prove that Parkin recruitment to mitochondria occurs in two steps: initially, Parkin interacts with Miro1 independently of ubiquitination at K572, and, in case of persistent mitochondrial damage, Parkin activity is amplified and results in further translocation of Parkin to the mitochondria.

Ca^{2+}-insensitive Miro1 is less ubiquitinated by Parkin

A recent X-ray crystal structure of Miro1 revealed that its cGTPase domain that includes lysine 572 forms an interface with its central EF-hand motif (Klosowiak *et al*, 2013, 2016), which is responsible for Ca^{2+} binding. From earlier findings, it is also known that Ca^{2+} binding decreases Miro1's affinity for binding partners involved in mitochondrial trafficking (MacAskill *et al*, 2009). We therefore speculated that the Miro1 EF-hand domain may also play a role in the Miro1-Parkin interaction. We studied whether the double substitutions of E208K and E328K in the Miro EF motifs (Miro1-EF), which abolish Ca^{2+} binding (Fransson *et al*, 2003), affected Parkin interaction with Miro1.

Figure 5A demonstrates that Miro1-EF still interacts with Parkin (both overexpressed and endogenous) but to a lesser extent than Miro1 WT. This was evident in both control conditions and when the cells were treated with A&O. In the Miro1 WT A&O-treated group, a number of higher molecular weight bands were positioned at approximately 9 and 20 kDa above Miro1 WT but no such bands were observed with Miro1-EF.

To ensure that the observed ladder represented an ubiquitinated form of Miro1, we co-expressed WT or EF Miro1 with EYFP-Parkin and ubiquitin-HA, immunoprecipitated the ubiquitin-HA and probed for Miro1. Again, several higher molecular forms of Miro1 WT were detected whereas in case of Miro1-EF, there was only one band visible (Fig 5B).

It was previously shown that phosphorylated ubiquitin acts as an activator of Parkin ligase activity (Koyano *et al*, 2014; Tang *et al*, 2017). We next confirmed our finding by reciprocal co-immunoprecipitation, where we co-expressed WT or EF Miro1 with EYFP-Parkin and probed for S65 phospho-ubiquitin. The results depicted in Fig 5C demonstrate that the higher molecular weight bands of Miro1 WT observed in the A&O-treated cells were recognised also by the phospho-ubiquitin (S65)-specific antibody but were absent in Miro1-EF-expressing cells. PINK1 is the major ubiquitin kinase to phosphorylate (and activate) Parkin, and as expected, overexpression of PINK1 led to massive phospho-ubiquitination of Miro1 WT (view the S65 phospho-ubiquitin-positive Miro1 bands) but this effect was significantly reduced in the case of Miro1-EF. S65 ubiquitin and Miro1 WT (inset in Fig 5C) match perfectly, showing that these higher molecular weight bands of Miro1 indeed represent Miro1-Ubi S65.

These results suggest that mutations in the EF-hands of Miro1 could make it less accessible for Parkin. Alternatively, conformational changes in Miro1-EF may block access of PINK1 to ubiquitinated Miro and prevent ubiquitin S65 phosphorylation.

Ca^{2+}-insensitive Miro1 inhibits Parkin translocation to mitochondria

Based on our findings, we hypothesised that Parkin cannot be stabilised on mitochondria if Miro1 EF-hands are mutated. Thus, we wondered if the Miro1-EF mutant could inhibit Parkin translocation to depolarised mitochondria. We performed a time-lapse microscopy experiment in separated compartments of the same dish allowing us to visualise different groups simultaneously. We followed EYFP-Parkin translocation in response to A&O treatment in control or Ca^{2+}-insensitive Miro1-EF mutant-expressing PC6 cells. Figure 6A demonstrates that the kinetics of EYFP-Parkin translocation from cytosol to mitochondria was significantly slower in EF-hands-mutated Miro1-expressing cells. Moreover, in Fig 6B, we found that fewer cells show EYFP-Parkin translocation to mitochondria in A&O-treated cells expressing Miro1-EF. The Miro1-EF mutant also suppressed PINK1-induced Parkin translocation to mitochondria (Fig 6C; note that Miro1-EF mutant overexpression alone did not induce Parkin translocation to mitochondria).

We repeated similar experiments in primary neurons. We used selective laser irradiation of individual mitochondria with a near-UV laser to demonstrate the translocation kinetics of EYFP-Parkin to damaged mitochondria (Choubey *et al*, 2011) in primary cortical neurons (Fig 6D). Laser-irradiation-induced Parkin translocation was PINK1 dependent, as it was completely suppressed when the

Figure 5. Ca^{2+}-insensitive Miro1 is less ubiquitinated in response to mitochondrial depolarisation.

A A Ca^{2+}-insensitive mutant of Miro1 (Miro1-EF) interacts with Parkin. HEK cells overexpressing myc-Miro1 or myc-Miro1-EF and EYFP-Parkin were treated with DMSO (control) or A&O (both 15 μM) for 3 h. Myc-Miro1 was immunoprecipitated and probes were immunoblotted for Miro1 (red) and Parkin (green). The high-contrast greyscale image from the green channel of this blot shows that endogenous Parkin co-immunoprecipitated with Miro1 in all conditions. The bar chart shows the quantification of co-immunoprecipitated Parkin EYFP from 4 different blots normalised to total EYFP-Parkin signal (*$P < 0.05$ and **$P < 0.01$, repeated-measures ANOVA).

B Miro1-EF is less susceptible to ubiquitination by Parkin. HEK cells overexpressing HA-ubiquitin, myc-Miro1 or myc-Miro1-EF and EYFP-Parkin were treated with DMSO (control) or A&O (both 15 μM) for 3 h. HA-ubiquitin was immunoprecipitated, and probes were immunoblotted for ubiquitin (red), Miro1 (green) and Parkin (green; representative images are from the same experimental material on separate SDS-PAGE-WB membranes). The high-contrast greyscale shows the green channel of this blot, and the bar chart shows quantification of co-immunoprecipitated Miro1 from 3 different blots (**$P < 0.01$ and ***$P < 0.001$, repeated-measures ANOVA). Note that EYFP-Parkin co-immunoprecipitated with ubiquitin only after A&O treatment.

C Mutation of Miro1 EF-hands diminishes Miro1 ubiquitination with S65-phosphorylated ubiquitin. HEK cells were transfected with EYFP-Parkin with either myc-Miro1-WT or myc-Miro1-EF with or without PINK1-V5. Cells were treated with either DMSO or A&O (both 10 μM) for 5 h with the exception of the PINK1-V5 group. Myc-Miro1 was immunoprecipitated and probes were immunoblotted for Miro1 (red), S65-phospho-ubiquitin and PINK1-V5 (green; the weak bands marked with the asterisk are nonspecific).

Data information: Data are presented as means ± SEM.
Source data are available online for this figure.

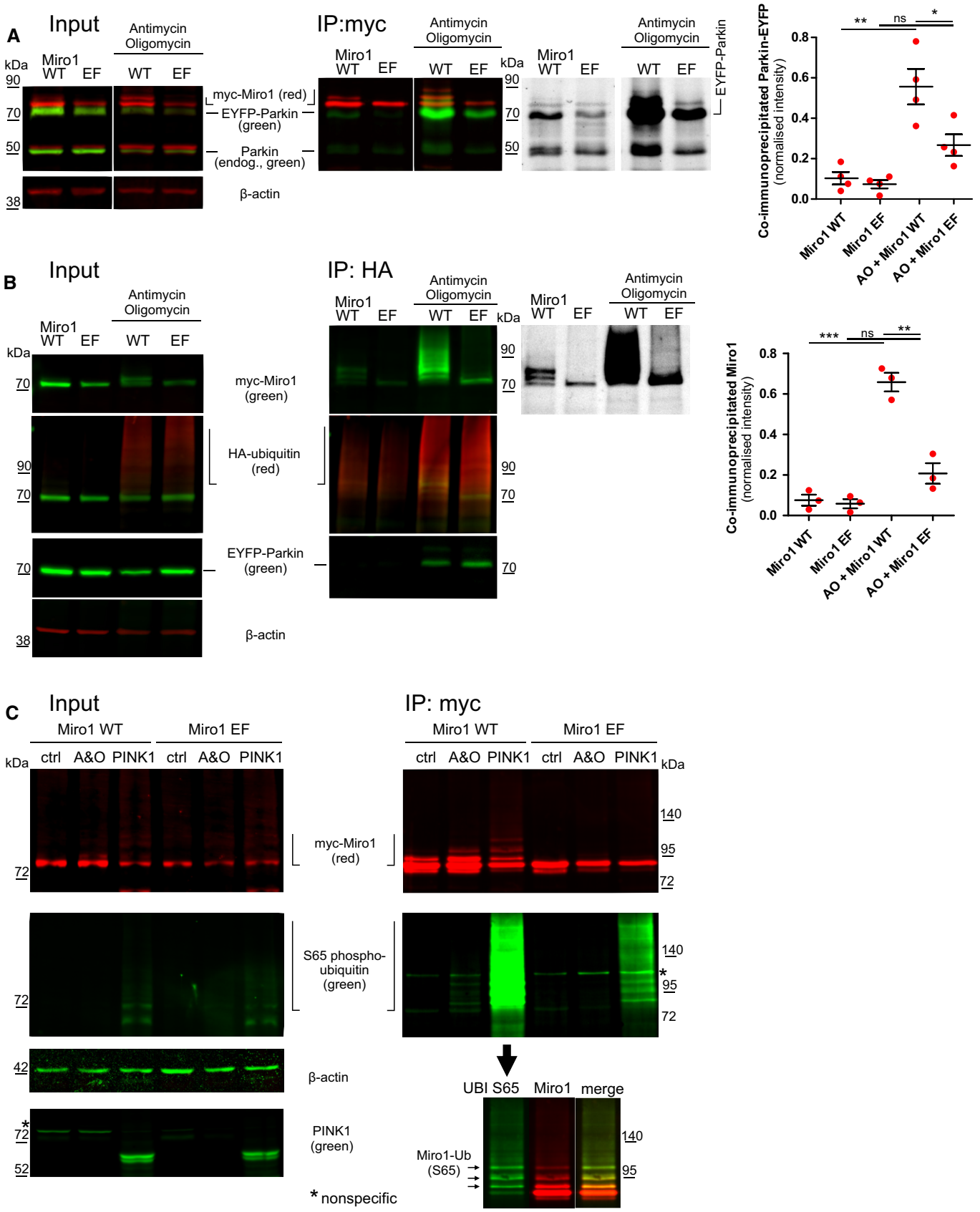
A
Input
Antimycin Oligomycin
Miro1 WT EF WT EF
kDa
90
70
50
38
myc-Miro1 (red)
EYFP-Parkin (green)
Parkin (endog., green)
β-actin
IP:myc
Antimycin Oligomycin
Miro1 WT EF WT EF
EYFP-Parkin
Co-immunoprecipitated Parkin-EYFP (normalised intensity)
**
ns
*
0.8
0.6
0.4
0.2
0.0
Miro1 WT
Miro1 EF
AO + Miro1 WT
AO + Miro1 EF
B
Input
Antimycin Oligomycin
Miro1 WT EF WT EF
kDa
70
90
70
70
38
myc-Miro1 (green)
HA-ubiquitin (red)
EYFP-Parkin (green)
β-actin
IP: HA
Antimycin Oligomycin
Miro1 WT EF WT EF
90
70
90
70
70
Co-immunoprecipitated Miro1 (normalised intensity)
***
ns
**
0.8
0.6
0.4
0.2
0.0
Miro1 WT
Miro1 EF
AO + Miro1 WT
AO + Miro1 EF
C
Input
Miro1 WT
Miro1 EF
ctrl A&O PINK1 ctrl A&O PINK1
kDa
72
72
42
72
52
myc-Miro1 (red)
S65 phospho-ubiquitin (green)
β-actin
PINK1 (green)
* nonspecific
IP: myc
Miro1 WT
Miro1 EF
ctrl A&O PINK1 ctrl A&O PINK1
kDa
140
95
72
140
*
95
72
UBI S65
Miro1
merge
Miro1-Ub (S65)
140
95

Figure 5.

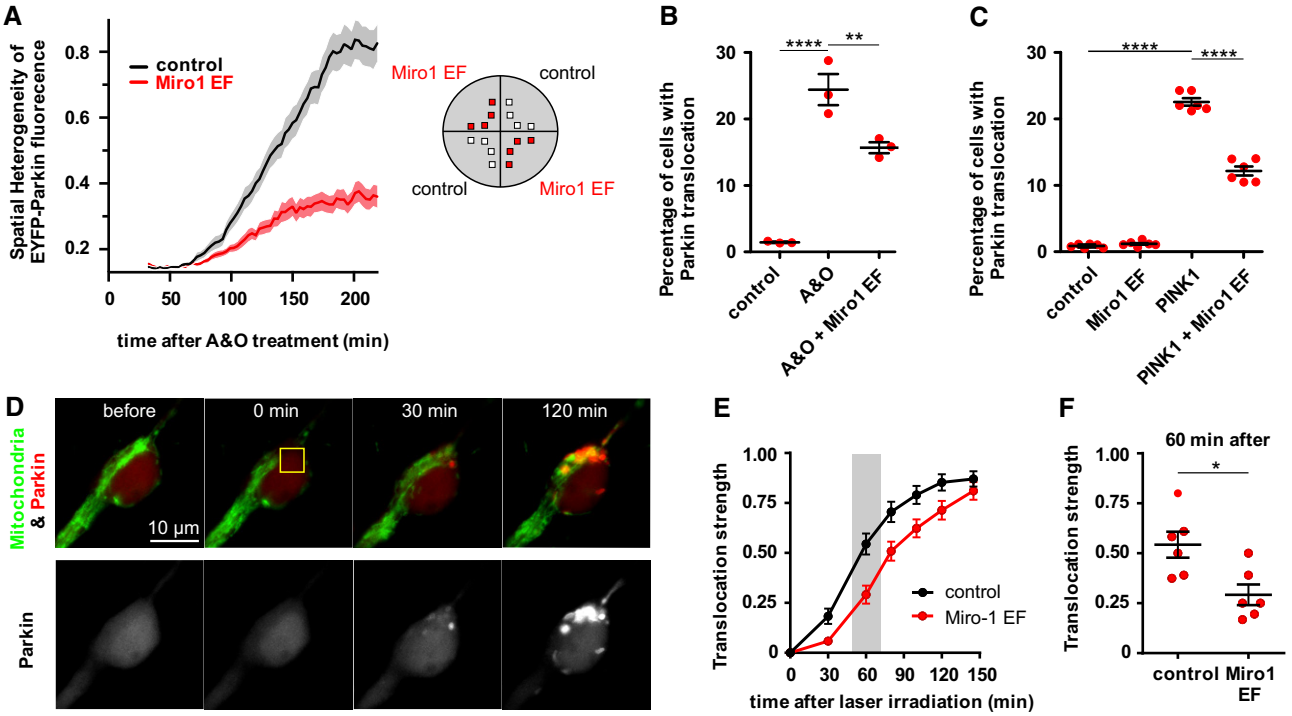

Figure 6. Ca^{2+}-insensitive Miro1 inhibits Parkin translocation to mitochondria.

A Kinetics of EYFP-Parkin translocation in response to A&O is different in control and Miro1-EF-expressing PC6 cells. The inset shows how different compartments of the same dish were transfected with EYFP-Parkin and control plasmid or Miro1-EF and followed over 3 h using a confocal microscope after addition of A&O (both 10 µM). The graph shows the average spatial heterogeneity of EYFP-Parkin fluorescence, reflecting the ratio of mitochondrial-to-cytosolic Parkin over time (n = 40–43 cells, difference between the curves $P < 0.0001$, two-way ANOVA; lines show mean, dashed area shows SEM).

B, C The percentage of cells where EYFP-Parkin translocates in response to A&O (both 10 µM, B) or PINK1 overexpression (C) is decreased in Miro1-EF-expressing PC6 cells. $^{**}P < 0.01$, $^{****}P < 0.0001$ compared with the indicated group (n = 3–6 dishes, 20 fields per dish, one-way ANOVA for B and Welch's ANOVA for C).

D Time course showing laser-induced EYFP-Parkin accumulation in the irradiated area of the neuronal soma of primary rat cortical neurons. Cells were transfected with CFP-mito and EYFP-Parkin and visualised using a confocal microscope. Mitochondria were irradiated in a 0.9 × 0.9 µm frame using a 405-nm laser line (25 iterations using 100% laser power, pixel time 164 µs).

E, F Miro1-EF delays and reduces irradiation-induced EYFP-Parkin translocation. (E) The time course of translocation strength in control and Miro1-EF-expressing neurons. Difference between the curves $P = 0.0016$, two-way ANOVA. (F) Comparison at the 60-min time point ($^{*}P < 0.05$, n = 6 dishes, at least 9 neurons per dish, t-test).

Data information: Data are presented as means ± SEM.
Source data are available online for this figure.

experiment was performed in neurons isolated from PINK1-deficient mice (none out of 18 studied neurons showed Parkin translocation). Also, no laser-induced Parkin translocation was observed when ligase-dead Parkin was used (0 out of 9). Finally, overexpression of Ca^{2+}-insensitive Miro1-EF decreased significantly the speed of Parkin translocation to irradiated mitochondria (Fig 6E and F).

Together, our results show that PINK1-dependent Parkin translocation in neuronal cells requires Miro1 to have intact Ca^{2+} sensing EF-hands.

Cytosolic Ca^{2+} levels affect Parkin translocation to mitochondria

Given the importance of the Ca^{2+}-sensitive EF-hands of Miro1 for Parkin translocation, we further tested whether cytosolic Ca^{2+} levels affected Parkin translocation to mitochondria in PC6 cells. First, we wondered whether Parkin translocation to depolarised mitochondria depended on Ca^{2+}. We followed EYFP-Parkin translocation in the presence of 1 mM Ca^{2+} or in Ca^{2+}-free conditions (in the presence of the Ca^{2+} chelator 5 µM BAPTA-AM, 30-min preincubation). Data depicted in Fig 7A show that A&O-induced Parkin translocation is significantly reduced in Ca^{2+}-free conditions. Further, treatment with the L-type Ca^{2+} channel agonist Bay K 8644 (5 µM, 30 min preincubation) to increase the Ca^{2+} influx to the cytoplasm accelerated Parkin translocation (Fig 7B). In the presence of Bay K 8644, Parkin translocation started considerably earlier and was faster. These results indicate that cytosolic Ca^{2+} is important for mitochondrial depolarisation-induced Parkin translocation.

We next tested whether pathological conditions that increase Ca^{2+} concentration could induce or affect Parkin translocation in neurons. We treated neurons for 10 min with 100 µM glutamate/10 µM glycine to activate ionotropic glutamate receptors and allow high levels of Ca^{2+} ions to enter the cell. Figure 7C and D demonstrates that glutamate treatment caused an immediate and excessive Ca^{2+} entry into the cytosol (measured using GCaMP7b) which was not affected by the overexpression of Miro1 EF or Miro1 WT. This

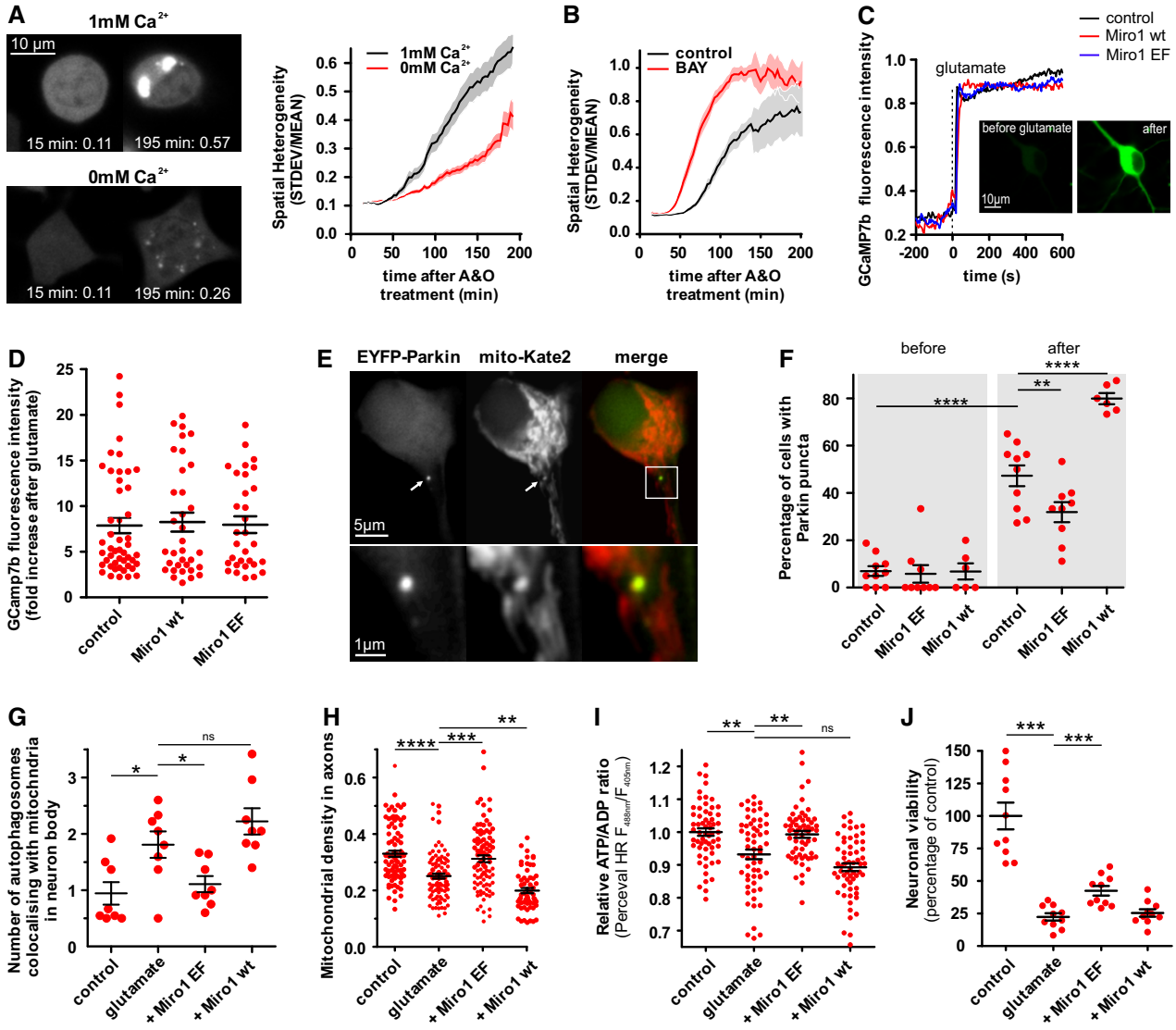

Figure 7. Glutamate-induced Ca^{2+} entry leads to Miro1-dependent Parkin translocation and mitophagy.

A EYFP-Parkin translocation requires Ca^{2+}. PC6 cells plated in separated compartments of the same dish maintained during the experiment in Krebs containing 1 mM Ca^{2+} or in Ca^{2+} free Krebs containing 5 µM BAPTA-AM were treated with A&O (both 10 µM). Images (left panels) demonstrate that EYFP-Parkin translocation was significantly weaker at zero Ca^{2+} at 195 min after A&O treatment (compared with 15 min; note the spatial heterogeneity values shown in photos). Spatial heterogeneity analysis (right panel) demonstrated that Parkin translocation was significantly decelerated in zero Ca^{2+} conditions (n = 25–27 cells; difference between the curves $P < 0.0001$, two-way ANOVA; lines show mean, dashed area shows SEM).

B EYFP-Parkin translocation accelerates in the presence of the L-type Ca^{2+} channel agonist Bay K 8644 (5 µM; n = 19–21 cells; difference between the curves $P < 0.0001$, two-way ANOVA; lines show mean, dashed area shows SEM).

C, D Treatment of neurons for 10 min with 100 µM glutamate/10 µM glycine led to excessive Ca^{2+} entry into the cytosol, visualised by increased cytosolic GCaMP7b fluorescence. Glutamate-induced Ca^{2+} entry was not affected by Miro1 WT or Miro1 EF overexpression; n = 31–48 neurons per group; ns, Kruskal–Wallis test).

E, F Glutamate treatment (100 µM glutamate/10 µM glycine for 10 min) led to the appearance of a few Parkin-positive strong puncta co-localising with mitochondrial marker (white arrow), imaged 2.5 h after treatment (E). Further analysis demonstrated that the expression of Miro1-EF mutant decreased and Miro1 WT increased the number of neurons with EYFP-Parkin-positive mitochondria following glutamate treatment (F; n = 6–10; $^{**}P < 0.01$ and $^{****}P < 0.0001$, one-way ANOVA).

G Glutamate treatment (100 µM glutamate/10 µM glycine for 10 min) was associated with an increased number of mitochondrial co-localisation with the autophagosome marker EGFP-LC3B in neuronal soma at 5–6 h later, which was not observed in Miro1-EF-expressing neurons (n = 8 dishes; $^{*}P < 0.05$, one-way ANOVA).

H Glutamate treatment (30 µM glutamate and 1 µM glycine for 10 min) was also associated with a significant loss of mitochondrial density in axons at 6 h later, which was reversed by Miro1-EF but not by Miro1 WT (n = 60–90 axons from 6 to 9 dishes; $^{**}P < 0.01$, $^{***}P < 0.001$ and $^{****}P < 0.0001$, Kruskal–Wallis test).

I Glutamate treatment (100 µM glutamate and 10 µM glycine for 10 min) led to a decline, at 6–8 h, in cytosolic ATP measured using ATP/ADP sensor Perceval HR, which was reversed by Miro1-EF but not by Miro1 WT (n = 59-60 neurons from 6 dishes; $^{**}P < 0.01$, Welch's ANOVA).

J Glutamate (100 µM glutamate and 10 µM glycine for 10 min) induced excitotoxicity (24 h after treatment) that was partially reversed by Miro1-EF but not by Miro1 WT. Data are presented as a percentage of control neuron count (n = 10 dishes; $^{***}P < 0.001$, repeated-measures ANOVA).

Data information: Data are presented as means ± SEM.
Source data are available online for this figure.

also led to a delayed increase in mitochondrial Ca^{2+}, measured using mitochondrial G-CEPIA1, which varied from cell to cell (Fig EV4A). Mitochondrial Ca^{2+} uptake leads in turn to mitochondrial depolarisation that was restored after glutamate was washed away (Fig EV4B and C). Nevertheless, when we imaged EYFP-Parkin 2.5 h later, we observed Parkin-positive mitochondria in glutamate-treated neurons (Fig 7E) suggesting that either some mitochondria remained depolarised or these mitochondria were more prone to damage.

Our findings suggested that Parkin cannot ubiquitinate the Miro1 EF-hand mutant. We speculated further that Ca^{2+} binding to Miro1 could be a prerequisite or at least a facilitating factor for its ubiquitination. It is known that Ca^{2+} binds to Miro1 EF-hands and causes an arrest of mitochondrial movement but such a conformational change might also facilitate Parkin translocation to mitochondria. First, we treated control, Miro1 WT- and Miro1-EF-expressing neurons with glutamate and followed their mitochondrial movement. As expected, the mitochondrial velocity decreased gradually, leading to almost complete arrest after 10 min of glutamate treatment. However, in Miro1-EF-overexpressing neurons, the mitochondrial motility was partly preserved, as has been previously described (Fig EV4D and E; MacAskill *et al*, 2009). Next, we speculated that Miro1-EF-overexpressing neurons could also have less Parkin translocation. Indeed, as demonstrated in Fig 7F, Miro1 EF-hand mutant suppressed glutamate-induced Parkin translocation in approximately half of treated neurons. In contrast, Miro1 WT overexpression enhanced Parkin translocation considerably. These changes cannot be explained by differences in recovery of mitochondrial membrane potential after glutamate treatment and washout as it was similar between groups (Fig EV4C). Thus, we conclude that Ca^{2+} binding to Miro1 not only regulates mitochondrial movement but may also be a switch for Parkin recruitment to mitochondria in (patho)physiological conditions.

We tested further whether these changes are also reflected at the level of mitophagy, which is downstream of Parkin translocation. Glutamate treatment led to a statistically significant twofold increase in the number of mitochondria co-localising with the autophagosome marker, EGFP-LC3B, in neuronal soma (Fig 7G). This effect was reversed by Miro1-EF but not by Miro1 WT. Similar trends were observed when measuring axonal mitochondrial density—glutamate treatment led to a significant loss in mitochondrial density/mass, which was reversed by Miro1-EF but not by Miro1 WT (Fig 7H). These lines of evidence suggest that excessive glutamate could trigger Ca^{2+}-dependent activation of mitophagy machinery with Ca^{2+} binding to Miro1 being a major step in this process.

Finally, we tested whether the above-described changes are sufficient to affect neuronal ATP levels and survival. We first estimated neuronal ATP/ADP ratio using the genetically encoded fluorescent ratiometric probe Perceval HR, which we have shown to be sufficiently sensitive to track intracellular ATP/ADP ratio in our model (Vaarmann *et al*, 2016). Glutamate treatment induced a clear and significant decrease in ATP levels that was reversed by the Miro1 EF and augmented by the Miro1 WT (Fig 7I). Miro1 EF but not Miro1 WT also improved viability after glutamate excitotoxicity (Fig 7J). Note that at control conditions both Miro1 WT and EF had no significant effect on ATP levels and viability (Fig EV5).

Discussion

Dysregulation of mitophagy is implicated in the pathogenesis of neurodegenerative diseases, such as Parkinson's disease, as well as metabolic diseases, heart failure, cancer and ageing. Parkin translocation to mitochondria is one of the earliest events determining the fate of unhealthy mitochondria, and better understanding of this process has major implications for health and disease.

This study identifies an additional step in this process. Herein, we show that a pool of Parkin already interacts with Miro1 before mitochondrial damage occurs. This interaction happens without PINK1, it does not involve Miro1 ubiquitination, and it does not disturb the function of Miro1 or mitochondria themselves. Moreover, this initial Parkin-Miro interaction plays a critical role after mitochondrial damage because knockdown of Miro proteins reduces Parkin translocation to mitochondria and suppresses mitophagic removal of mitochondria. We also demonstrate that calcium and calcium-sensing Miro1 EF-hand domains play a relevant role in these events. Mutations in the EF-hands decrease Parkin recruitment to damaged mitochondria, reduce ubiquitination of Miro1 and decrease calcium-provoked mitophagy in neurons. Together, our results suggest that Miro1 functions as a calcium-sensitive regulatory docking site for Parkin on mitochondria.

The disturbance of mitophagy in Miro-deficient cells was surprising, as Miro proteins comprise only a small fraction of Parkin substrates on mitochondria (Sun *et al*, 2012; Martinez *et al*, 2017). Parkin is also shown to ubiquitinate VDAC isoforms, Mfn1 and 2 and Tom20 as well as Cisd1 and 2 (Chan *et al*, 2011; Lazarou *et al*, 2013; Sarraf *et al*, 2013; Martinez *et al*, 2017), and the loss of only one of the less abundant substrates should not have such a profound effect on downstream events as we demonstrated in our experiments. However, recent data suggest that although Miro deletion affects mitochondrial distribution and motility, the mitochondria retain functionality and membrane potential (Nguyen *et al*, 2014; López-Doménech *et al*, 2016) indicating that the loss of Miro *per se* does not cause mitochondrial depolarisation (Fig 2E), which is one of the major causes of mitochondrial removal. In line with our results, Chen *et al* (2017) showed recently that loss of Miro1 selectively in pancreatic beta cells inhibited mitophagy *in vivo*.

Further, we found that Miro1, without PINK1, is sufficient to recruit a small proportion of Parkin to mitochondria. Of relevance, we observed Parkin on healthy, polarised mitochondria which retained their motility. Previously, overexpression of EYFP-Parkin has been shown to suppress time in motion of mitochondria in axons from hippocampal neurons without affecting their velocity (Wang *et al*, 2011). However, in cortical neurons overexpressing Parkin-HA together with Miro1, we were unable to find any inhibitory effect on mitochondrial trafficking (we carried out manual, blinded analysis of more than 600 mitochondria per group from 4 independent cultures).

We found that overexpression of Parkin does not affect Miro1 levels indicating that the "initial" pool of Parkin associated with Miro1 is unlikely to disturb Miro1 function and stop mitochondrial motility. Parkin co-expression induced Miro1 (mono)ubiquitination even in basal conditions, which might exert an additional role in the regulation of mitochondrial motility. Although speculative, this suggestion has been previously proposed by Klosowiak *et al*, 2016.

Miro proteins have been shown to be targeted by Parkin for ubiquitination and proteasomal degradation upon mitochondrial depolarisation (Wang *et al*, 2011; Liu *et al*, 2012; Sarraf *et al*, 2013; Birsa *et al*, 2014). Here, we confirmed increased interaction between Miro1 and Parkin and ubiquitination of Miro1 in response to the mitochondrial toxins antimycin and oligomycin, but we were also able to detect an interaction between Miro1 and Parkin in basal conditions. Miro1 was also able to interact with the E3 ligase-deficient Parkin mutants T240R and C431N (Fig 3D). Thus, we suggest that the Miro1-Parkin interaction occurs prior to the amplification of the PINK1-ubiquitin-Parkin cascade. When acute damage persists, Miro1 is degraded by "full scale" activation of the Parkin-dependent pathway that requires both PINK1 and the ligase activity of Parkin and leads to polyubiquitination of Miro1.

These findings allow us to speculate that Miro1 could serve as a mitochondrial "docking station" or receptor for inactive Parkin that facilitates its recruitment to depolarised mitochondria. It has been suggested that inactive, cytosolic Parkin is continuously sampling the mitochondrial surface via a diffusion-controlled process (Ordureau *et al*, 2014) but on the other hand it has also been proposed that some of the Parkin substrates may serve as mitochondrial docking sites that accelerate the recruitment of Parkin from the cytosol (Sun *et al*, 2012). For example, it has been shown that in the absence of all three VDAC isoforms, the recruitment of Parkin to defective mitochondria and their subsequent mitophagy is impaired (Sun *et al*, 2012). Recently, it was shown that pre-existing phosphorylated ubiquitin recruits Parkin to mitochondria, whereas phospho-ubiquitin binding precedes Parkin phosphorylation by PINK1, which, in turn, leads to E3 ligase activation (Shiba-Fukushima *et al*, 2014; Okatsu *et al*, 2015; Tang *et al*, 2017). Our finding that Miro1 can interact with Parkin also at basal conditions, e.g., without stabilised PINK1, makes Miro1 the most likely candidate for an initial dock for inactive Parkin. The latter is indirectly supported by evidence showing that PINK1 interacts with Miro1 (Weihofen *et al*, 2009; Wang *et al*, 2011) and that Miro1 can stabilise phosphomimetic Parkin on the outer mitochondrial membrane (Birsa *et al*, 2014). This docking theory explains many of our observations, such as delayed Parkin translocation after loss of Miros and Miro1-overexpression-induced Parkin translocation. Thus, based on our results, we speculate that Miro1 initiates Parkin recruitment, which is amplified by PINK1 upon mitochondrial depolarisation. Similar to Miro1, Miro2 also recruited Parkin to mitochondria suggesting that Miro proteins act redundantly in this process.

We also demonstrate that ubiquitination of Miro1 happens only when its Ca^{2+} sensing EF-hands are functional: Parkin did not polyubiquitinate Miro1 when its EF-hands were mutated (Fig 5). Moreover, this mutant showed a partial negative dominant effect as it suppressed partially Parkin translocation to mitochondria induced by very different settings—by PINK1 overexpression, by oligomycin and antimycin treatment and by laser-induced mitochondrial damage (Fig 6). A recent X-ray crystal structure of Miro1 revealed that Parkin targets lysine in the C-terminal GTPase domain, which forms an interface with the central EF-hand (Klosowiak *et al*, 2013, 2016). Modification of the EF-hands might cause a structural constraint preventing access of Parkin to lysine K572 or blocking PINK1 from phosphorylating the ubiquitins on Miro1. PINK1 phosphorylates ubiquitin on a Parkin substrate (or Parkin phospho-ubiquitinates its substrate) after mitochondrial depolarisation and PINK1 accumulation. Ubiquitination of Miro1 with S65-phosphorylated ubiquitin has been shown previously in *in vitro* ubiquitination assays (Kazlauskaite *et al*, 2014b, 2015; Ordureau *et al*, 2015) but not in cellular systems.

The Ca^{2+}-insensitive Miro1 EF-hand mutant also suppressed Parkin translocation in response to glutamate treatment. Transient glutamate exposure induces Ca^{2+} influx into the cytosol leading to mitochondrial Ca^{2+} uptake and depolarisation of the inner mitochondrial membrane (Schinder *et al*, 1996; White & Reynolds, 1996). This depolarisation appears to be sufficient to induce weak Parkin translocation. In our hands, the effect of glutamate on Parkin translocation was stronger in Miro1 WT-overexpressing cells and significantly suppressed when Miro1 EF-hands were mutated. Thus, our data suggest that Parkin translocation might involve Ca^{2+} binding to Miro1 EF-hands. Significantly, the Miro1 EF-hand mutant also protected neurons from glutamate-induced mitophagy, ATP loss and neuronal death, showing the relevance of this phenomenon to brain pathologies involving excitotoxicity.

It has been suggested that cytosolic Ca^{2+} levels are one of the factors contributing to mitophagy (East & Campanella, 2013; Rimessi *et al*, 2013). For example, MacVicar *et al* (2015) demonstrated that treatment with the Ca^{2+} chelator BAPTA-AM blocked CCCP-induced mitophagy and suggested that transient and local Ca^{2+} spikes might be needed for mitophagy. Cherra *et al* (2013) demonstrated that excess cytosolic Ca^{2+} is associated with profound mitophagy and that restoring Ca^{2+} homeostasis through Ca^{2+} chelation or inhibition of voltage-gated Ca^{2+} channels was sufficient to prevent the mutant *LRRK2* phenotype related to Parkinson disease.

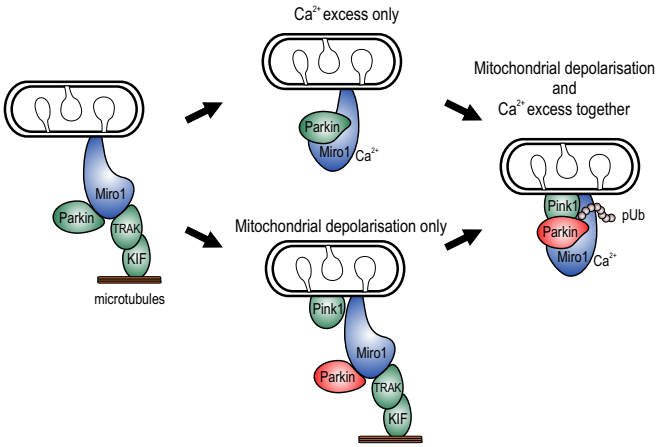

Figure 8. Miro1 as a calcium-dependent safety switch for Parkin recruitment to mitochondria.

Depolarisation of the mitochondrial membrane stabilises Pink1 in the outer membrane. However, without calcium, Miro remains protected and cannot be ubiquitinated by Parkin. Calcium binding to Miro1 EF-hands removes the structural constraint preventing access of Parkin to its preferred lysine(s) or/and enables the phosphorylation of ubiquitin(s) on Miro. This amplifies the Parkin activation cycle and ensures faster Parkin translocation to mitochondria.

We have recently demonstrated that increased cytosolic Ca^{2+} levels are associated with profound mitophagy in Wolfram syndrome 1-deficient neurons (Cagalinec *et al*, 2016). Current findings allow us to speculate that Miro proteins may also play a significant role in that process. At high cytosolic Ca^{2+} levels, Ca^{2+} ions bind Miro1 EF-hands leading to an uncoupling of mitochondria from microtubules (MacAskill *et al*, 2009; Wang & Schwarz, 2009), thus positioning mitochondria to ensure local energy supply. Here, we show that calcium binding is also required for Parkin-mediated Miro1 ubiquitination and contributes to the activation of mitophagy machinery. Thus, Miro1 may function as a calcium-dependent safety switch that accelerates Parkin recruitment to mitochondria when the mitochondrion is detached from the microtubule (Fig 8).

Materials and Methods

Media and reagents

Reagents were from the following manufacturers: 35-mm glass-bottomed dishes (MatTek, P35G-1.0-14-C), CELLview™ dishes (Greiner Bio-One 627 871), poly-L-lysine (Sigma-Aldrich, P6282), collagen IV (Sigma-Aldrich, C5533), penicillin, streptomycin and amphotericin B (Invitrogen, 15240-096), gentamicin (Krka, d. d., Novo Mesto, Slovakia), RPMI-1640 (Life Technologies, A1049101), DMEM (Life Technologies, 31966021), Neurobasal™ A (Life Technologies, 10888022 and 12349015 (without phenol red)), HBSS 1640 (Life Technologies, 14025050), BME (Life Technologies 41010-109), Opti-MEM I (Life Technologies, 31985-047), B-27® Supplement (50X, serum free, Life Technologies, 17504044), foetal bovine serum (Life Technologies, 10270106), horse serum (Life Technologies, 26050088), GlutaMAX™-I (Life Technologies, 3505038) Lipofectamine® 2000 (Invitrogen, 11668-019), Metafectene® (Biontex Laboratories GmbH, T040), DMSO (Sigma-Aldrich, 472301), FCCP (Tocris, 0453), G418 (Sigma-Aldrich, A1720), MG132 (Tocris, 1748), protease inhibitor cocktail cOmplete (Roche, 04693116001), protein G-sepharose 4B beads (Invitrogen, 101243), DC Protein Assay reagent (Bio-Rad, 500-0111), Pierce Lane Marker Reducing sample buffer (Thermo Fisher Scientific, 39000).

Plasmids

Plasmids expressing scrambled shRNA or shRNAs against mouse RHOT1 (KM35868N, suppresses efficiently also rat RHOT1), rat RHOT2 (KR44228N) and rat PINK1 (KR55105N) were from SABiosciences and validated earlier (Cagalinec *et al*, 2013; Choubey *et al*, 2014). Plasmids expressing mitochondrial DsRed2 (632421), mitochondrial CFP (632432) and EGFP (6085-1) were from Clontech, untagged Miro2 (SC127208) from Origene and mKate2-mito (FP187) from Evrogen. Mito-Keima was from Amalgaam (AM-V0251), and mito-KikGR1 was constructed as described earlier (Cagalinec *et al*, 2013). EGFP-LC3B (24920), HA-ubiquitin (18712), PINK1-V5 (13320), HA-Parkin (17613), Perceval HR (49082), pAAV-hSyn-DsRedExpress (22907), GCaMP7b (104489) and Cepia3mt (58219) were obtained from Addgene (Cambridge, MA). EYFP-Parkin and EYFP-Parkin C431N were from Dr. R. Youle, untagged PINK1 from Dr. E. Deas, GCamp6 from G. Szabadkai and Prk5-myc-Miro1, myc-Miro2 and EGFP-Miro1 from Dr. P. Aspenström. EYFP-Parkin point mutation T240R and Miro1 point mutations were generated by Mutagenex Inc. (Hillsborough, NJ, USA).

Cell cultures

Primary rat neuronal cultures were prepared from < 1-day-old neonatal Wistar rats as described earlier (Cagalinec *et al*, 2013). Neurons in BME supplemented with 10% FBS, 2 mM GlutaMAX™-I and 100 μg/ml gentamicin were plated onto 35-mm glass-bottomed dishes (MatTek, MA, USA), which were pre-coated with poly-L-lysine, at a density of 10^6 cells per dish in 2 ml of cell suspension. After incubating for 3 h, the medium was changed to Neurobasal™ A medium containing B-27® supplement, 2 mM GlutaMAX™-I and 100 μg/ml gentamicin. PC6 cells were grown in RPMI-1640 medium supplemented with 10% horse serum and 5% FBS on collagen IV-coated 100-mm plastic dishes or on 35-mm glass-bottomed dishes. HEK293 cells were cultured in DMEM containing GlutaMAX™-I supplemented with 10% FBS. Mouse embryonic fibroblasts were isolated from wild-type and *PINK1*-deficient mice (C57Bl/6J and B6;129-*PINK1*^{tm1Aub}/J; Jackson Laboratories). MEF cells were cultured in DMEM containing 2 mM GlutaMAX™-I, supplemented with 10% FBS and a 1% solution of penicillin and streptomycin.

Transfection

Primary cortical neurons were transfected at DIV2–3 (with exception of glutamate experiments where neurons were transfected at DIV5–7). For transfection of cells growing on glass-bottomed dishes, the conditioned medium was replaced with 100 μl Opti-MEM I medium containing 2% Lipofectamine® 2000 and 1–2 μg of total DNA with an equal amount of each different plasmid. The dishes were incubated for 3–4 h, after which fresh medium was added. Similar to neurons, PC6 cells and MEFs growing in glass-bottomed dishes were transfected 1 day after plating (except that 5% Metafectene was used instead of Lipofectamine).

For biochemical analyses, HEK and PC6 cells were transfected in 60-mm plastic dishes. Medium was replaced with 2 ml of Opti-MEM I medium containing 0.5% Lipofectamine® 2000 and 10 μg of total DNA with an equal amount of each plasmid. After 3–4 h, fresh medium was added. For experiments with shRNA-expressing plasmids that also contained a neomycin resistance gene (shRNA efficiency testing), the PC6 cell medium was supplemented with 200 μg/ml G418 for 6–7 days.

In all cases where specific shRNAs were transfected, the same amount of scrambled shRNA was transfected into the control group (s). In the case of overexpression of empty vector, EGFP/YFP or firefly luciferase was used to compensate in control groups. The expression levels of PINK1, Parkin and Miro proteins were validated by immunofluorescence (Appendix Fig S2).

Co-immunoprecipitation

Three hours before co-immunoprecipitation experiments, HEK cells were treated with 25 μM MG132 and with DMSO or 15 μM antimycin and oligomycin supplemented in conditioned medium. We carried out numerous experiments with and without MG132 and found that Miro1 and Parkin interaction does not depend on the presence of MG132. For immunoprecipitation, the HEK cells were

washed with ice-cold PBS and pelleted at 800 *g* for 5 min at 4°C and then lysed in ice-cold IP lysis buffer containing 20 mM HEPES, 100 mM NaCl, 5 mM NaEDTA, 1% Triton X-100, 10% glycerol, pH 7.4, and protease inhibitor cocktail. Cell lysates were passed through a 26-G needle 10 times before incubating on ice for 30 min with shaking at 350 rpm. The insoluble fraction was removed by centrifugation at 30,000 *g* for 15 min at 4°C and then at 55,000 *g* for 15 min at 4°C. The protein concentrations were estimated using Bio-Rad DC™ Protein Assay reagent according to the manufacturer's protocol. Lysates (750–1,000 μg of protein) were incubated overnight on a rotary shaker at 4 °C in Pierce spin columns with mouse anti-MYC (Invitrogen, 46-0603; 1:400), rabbit anti-HA (Abcam, ab9110; 1:200), mouse anti-RHOT1 (Atlas, AMAb90852; 1:100) or rabbit anti-RHOT2 (Proteintech 11237-1-AP; 1:500) antibodies. The following morning 100 μl protein G-sepharose 4B beads (50% suspension in IP lysis buffer) were added and samples further incubated for 3 h on a rotary shaker at 4°C. Beads were then washed 5 times with IP lysis buffer, and immunoprecipitates were eluted in 80 μl of diluted (2×) Pierce Lane Marker Reducing sample buffer at 99°C for 10 min followed by centrifugation for 10 min at 20,000 *g* at room temperature.

Western blotting

Total cell lysates were obtained by solubilisation in RIPA buffer containing protease inhibitor followed by centrifugation at 30,000 *g* for 15 min at 4°C. RIPA-solubilised total cell lysates, inputs and elutes from immunoprecipitation experiments were analysed using Western blotting (WB). Equivalent amounts of proteins were resolved on 8 or 10% polyacrylamide gels by SDS-PAGE. Resolved proteins were transferred to Immobilon®P^{SQ} membrane (ISEQ00010, Millipore) in 0.1 M Tris-base, pH 8.3, 0.192 M glycine and 10% (v/v) methanol using an electrophoretic transfer system with cold-block. The membranes were blocked in Odyssey blocking buffer (LI-COR Bioscience, 927-40000) at room temperature for 1 h. After blocking, the membranes were incubated sequentially overnight with different primary antibodies based on the requirement of the experiment. Antibody dilutions used were rabbit anti-RHOT1 (Miro1) 1:1,000 (recognising both Miro1 and Miro2, Atlas, HPA010687), rabbit anti-RHOT2 1:1,000 (Proteintech, 11237-1-AP), rabbit anti-PINK1 1:1,000 (Atlas, HPA001931), rabbit anti-PARK2 (Abcam, ab15954) 1:1,000, rabbit anti-MYC 1:2,000 (Abcam, ab9106), mouse anti-MYC 1:2,000 (Invitrogen, 46-0603), mouse anti-β actin 1:5,000 (Sigma-Aldrich, A2228), goat anti-ubiquitin (Abcam, ab9134), rabbit anti-S65-ubiquitin 1:500 (Bio-Techne, A-110), rabbit anti-V5 1:1,000 (Abcam, ab15828), mouse anti-GFP 1:2,000 (Abcam, ab1218) and rabbit anti-GFP 1:5,000 (Abcam, ab290). Incubations were followed by washing and incubation with goat anti-rabbit IRDye 800CW (926-32211) or 680LT (926-68021), goat anti-mouse IRDye 800CW (926-32210) or 680LT (926-68020) or donkey anti-goat IRDye 680RD (926-68074) (all 1:5,000, all from LI-COR Bioscience) for 1 h at room temperature. Immunoreactive bands and molecular weight were detected using the Odyssey Infrared Imaging System (LI-COR Bioscience, Lincoln, NE, USA).

Parkin translocation

PC6 cells and MEFs transfected with WT EYFP-Parkin, T240R EYFP-Parkin or C431N EYFP-Parkin and plasmids of interest were co-transfected with PINK1 or treated with 10 μM of both antimycin and oligomycin or with DMSO for 3 h. Cells were visualised before and after treatment using an Olympus IX70 inverted microscope (Tokyo, Japan) equipped with a WLSM PlanApo 40×/0.90 water immersion objective and Olympus DP70 CCD camera (Tokyo, Japan). For each experimental condition, at least 20 fields per dish from 3 to 11 dishes were randomly captured for further analysis of the percentage of cells showing EYFP-Parkin translocation.

Primary cortical neurons transfected at DIV5–7 were treated 10 min with 100 μM glutamate/10 μM glycine in HBSS at DIV9–10, the glutamate was then washed away and the neurons visualised in Neurobasal™ A medium without phenol red 2.5 h later using a 514 laser line of LSM 510 confocal microscope (Plan-Apochromat 63×/1.4 oil immersion objective). For each experimental condition, approximately 10 neurons per dish from 4 to 9 dishes per condition were randomly captured and the percentage of neurons showing EYFP-Parkin translocation was calculated.

Kinetics of Parkin translocation

To measure the kinetics of Parkin translocation, the PC6 cells were plated in collagen IV-coated 35-mm CELLview™ dishes subdivided into four individual compartments to allow simultaneous analysis of various treatments and diverse transfections. Cells were transfected 1 day after plating with EYFP-Parkin and plasmids of interest and visualised 3–4 days later using a 514 nm laser line of LSM 780 confocal microscope (Plan-Apochromat 63×/1.4 oil immersion objective). Conditioned media was first replaced with fresh media or Krebs–Ringer solution, and the compartments were then treated with 10 μM of both antimycin and oligomycin. At least 4 randomly selected fields (134.7 × 134.7 μm) from each compartment were then simultaneously imaged at 3 min intervals over at least 200 min. The temperature (37°C), humidity and CO_2 levels were maintained using a climate chamber. We then quantified the spatial heterogeneity (coefficient of variation of the intensity of individual pixels) of EYFP-Parkin signal from individual cells for each time point using ImageJ. Spatial heterogeneity was relatively low when EYFP-Parkin was homogeneously cytosolic and reached close to one when the majority of cytosolic EYFP-Parkin translocated to mitochondria.

Laser-irradiation-induced Parkin translocation

For laser-irradiation-induced Parkin translocation, the primary cortical neurons were transfected at DIV2 with EYFP-Parkin and plasmids of interests. 3–4 days later, growth media were replaced with Krebs–Ringer solution supplemented with 1 mM Ca^{2+}. Randomly selected neuronal cell bodies (approximately ten from each dish) were visualised using a 514 nm laser line of LSM 510 confocal microscope (Plan-Apochromat 63×/1.4 oil immersion objective) and a sub-population of mitochondria were then irradiated with a 405 nm laser line (ROI size 0.9 × 0.9 μm), and images were collected simultaneously from these neurons at 30-min intervals over at least 150 min. The temperature (37°C), humidity and CO_2 levels were maintained using a climate chamber. The strengths of EYFP-Parkin translocation was evaluated using a scale from 0 to 1, based on the size, amount and location of EYFP-Parkin dots in the cell body (0—no translocation, 0.25—weak translocation, small dot in the area of laser irradiation, 0.5—clear translocation in the area

of laser irradiation, 0.75—large translocation in the area of laser irradiation, several smaller and bigger EYFP-Parkin dots, 1—massive full translocation, EYFP-Parkin dots are located all over the soma). For each experimental condition, approximately 10 neurons per dish from 6 dishes per condition were randomly captured.

Mitochondrial trafficking and mitochondrial density

For mitochondrial movement analysis, primary cortical neuronal cultures were transfected with mito-KikGR1 plasmid or mito-Kate2 and plasmids of interest and examined at DIV5–7 (in Miro1 and Parkin overexpression experiments), DIV7–9 (in Miro shRNA and Syntaphilin experiments) or DIV9–12 (glutamate experiments) using a 488 or 564 nm laser line of LSM 780 confocal microscope (C-Apochromat 63×/1.2 water immersion objective). For image acquisition, the images were taken at 10-s intervals for 10 min. The temperature (37°C), humidity and CO_2 (5%) levels were maintained using a climate chamber. In glutamate experiment, neurons were treated with 30 μM glutamate/1 μM glycine in HBSS and imaged 5 min before and 10 min after glutamate treatment. The movement of mitochondria was manually tracked throughout the time lapse (using Retrac version 2.10.05) from at least 4 axons per dish from at least 4 dishes per condition (in Miro shRNA, or Miro1 and Parkin overexpression experiments) and from 1 axon per dish from at least 4 dishes per condition (glutamate treatment experiments) and analysed further using an in-house Excel macro. Time in anterograde or retrograde motion for individual mitochondria was calculated by dividing the time spent in anterograde or retrograde movement by the total observation time. Anterograde or retrograde movement velocities for individual mitochondria were calculated by dividing the distance they moved by the total observation time. Total time in motion was calculated by summarising anterograde and retrograde motilities. The fraction of moving mitochondria was calculated as the percentage of moving mitochondria during each 10-min experiment for each studied axon.

For mitochondrial density measurements, the neurons were transfected at DIV6–7 with EGFP, mitochondrial pDsRed2 and plasmids of interest. At DIV9–10, the neurons were treated for 10 min with 30 μM glutamate/1 μM glycine in HBSS, and axons from randomly selected neurons were visualised 6 h later using an Olympus IX70 inverted microscope (WLSM PlanApo 40×/0.90 water immersion objective). For each experimental condition, at least 10 axons per dish from at least 4 dishes were randomly captured. Mitochondrial length measurements were performed as described previously (Cagalinec *et al*, 2013).

Mitophagy assays

PC6 cells were transfected at 1 day after plating with mitochondrially targeted Keima plus scrambled shRNA or Miro shRNAs and plasmids of interest and were imaged on DIV4. The excitation spectrum of Keima shifts from 440 to 586 nm when mitochondria are delivered to acidic lysosomes, which enables quantification of mitophagy. Images were acquired using a LSM 510 laser-scanning confocal microscope (LCI Plan-Neofluar 63×/1.3 water immersion objective) using the laser lines 458 nm (mitochondria at neutral pH) and 561 nm (mitochondria under acidic pH), and the 561–458 nm signal ratio was measured using ImageJ.

Primary cortical neurons were transfected at DIV2 with mitochondrial Keima and scrambled or Miro1 and Miro2 shRNAs and images were acquired at DIV7, and the mitochondria in lysosomes were counted manually by a blinded observer. In another set of experiments, neurons were transfected similarly with pEGFP-LC3B, mKate2-mito and scrambled or Miro1 and Miro2 shRNAs and the number of mitochondria co-localising with the autophagosome marker was counted.

For glutamate experiments, primary cortical neurons were transfected at DIV6–7 with pEGFP-LC3B, mKate2-mito and plasmids of interest, treated with 100 μM glutamate/10 μM glycine for 10 min at DIV11–12, and co-localisation of EGFP-LC3 dots with mitochondrial mKate2-mito was visualised 5–6 h later on LSM 510 (LCI Plan-Neofluar 63×/1.3 water immersion objective) and counted by a blinded observer.

Mitochondrial membrane potential and calcium measurements

For mitochondrial membrane potential measurements, primary cortical neurons transfected with Miro1 WT, Miro1-EF and cytosolic GFP to visualise transfected cells were maintained in Hank's balanced salt solution (HBSS with Ca^{2+} and Mg^{2+}) containing 5 nM TMRE dissolved in DMSO and incubated at 37°C for 40 min. 100 μM glutamate and 10 μM glycine were then added for 10 min after which cells were washed out with HBSS containing TMRE. Neurons were imaged during the glutamate treatment and after washout using 488 nm and 561 nm laser lines of LSM 780 confocal microscope (Plan-Apochromat 40 × 1.3 oil immersion objective), and emitted fluorescence was recorded at 40-s intervals. TMRE signal from non-transfected or transfected individual neurons was measured using ImageJ.

To visualise cytosolic or mitochondrial Ca^{2+}, primary cortical neurons were transfected with GCaMP7b or mitochondrial G-CEPIA1, respectively. 3–4 days later, the Neurobasal™A medium was replaced by HBSS with Ca^{2+} and Mg^{2+} and 100 μM glutamate and 10 μM glycine were used to elicit Ca^{2+} transients. The emitted fluorescence was recorded at 30-s intervals using a LSM 780 confocal microscope (488 nm line, Plan-Apochromat 63 × 1.4 oil immersion objective).

ATP/ADP ratio measurements and neuronal survival

Neuronal somas expressing the ATP/ADP ratio sensor Perceval HR were excited using a 405-nm diode laser and a 488-nm line of an Argon laser, and emission was collected using a 494–553-nm window (Vaarmann *et al*, 2016). Data are expressed as the ratio of fluorescence emission from neuronal soma evoked by 488 nm excitation/405 nm excitation (F488 nm/F405 nm).

In neuronal survival experiments, neurons expressing neuron-specific pAAV-hSyn-DsRed1 were counted manually from 50 fields per dish by two observers.

Statistics

Data are presented as the mean ± SEM or Tukey boxplot. The D'Agostino-Pearson omnibus test was used to test the normality of distribution. To test equality of variances, we used the *F* test for two conditions or Brown and Forsythe test for more than two conditions. Student *t*-tests, Mann–Whitney *U*-tests, one-way

ANOVA and repeated-measures ANOVA followed by Sidak post hoc test, Welch's ANOVA followed by Games–Howell test, or Kruskal–Wallis tests followed by the Dunn test were used to compare differences between experimental samples and control groups. Two-way ANOVAs were used to analyse interactions between two factors. *P*-values of < 0.05 were considered statistically significant.

Expanded View for this article is available online.

Acknowledgements
We thank Dr. R. Youle, Dr. G. Szabadkai, Dr. E. Deas, Dr. P. Apenström for providing the plasmids used in this study. We thank Ulla Peterson for her preparation of primary neurons. This work was supported by grants from the Estonian Research Council (IUT2-5), the European Regional Development Fund (Project No. 2014-2020.4.01.15-0012) and from the European Union's Horizon 2020 research and innovation programme under grant agreement 692202. D.S. was supported by the grant ETF8810 from Estonian Science Foundation and V.C. by grant PUT513 from the Estonian Research Council.

Author contributions
DS and AK conceived and designed the project; DS, MK, VC and AK designed experiments; DS, MK, VC, NG, JL, MAH, MC, MM, AZ, ML and AK performed and analysed experiments; DS, MK, MAH and AK provided reagents; DS and AK wrote the manuscript; all authors reviewed and edited the manuscript; DS, VC and AK secured funding.

Conflict of interest
The authors declare that they have no conflict of interest.

References

Babic M, Russo GJ, Wellington AJ, Sangston RM, Gonzalez M, Zinsmaier KE (2015) Miro's N-terminal GTPase domain is required for transport of mitochondria into axons and dendrites. *J Neurosci* 35: 5754 – 5771

Bingol B, Tea J, Phu L, Reichelt M, Bakalarski C, Song Q, Foreman O, Kirkpatrick D, Sheng M (2014) The mitochondrial deubiquitinase USP30 opposes parkin-mediated mitophagy. *Nature* 510: 370 – 375

Birsa N, Norkett R, Wauer T, Mevissen T, Wu H, Foltynie T, Bhatia K, Hirst W, Komander D, Plun-Favreau H, Kittler J (2014) Lysine 27 ubiquitination of the mitochondrial transport protein miro is dependent on serine 65 of the parkin ubiquitin ligase. *J Biol Chem* 289: 14569 – 14582

Cagalinec M, Safiulina D, Liiv M, Liiv J, Choubey V, Wareski P, Veksler V, Kaasik A (2013) Principles of the mitochondrial fusion and fission cycle in neurons. *J Cell Sci* 126: 2187 – 2197

Cagalinec M, Liiv M, Hodurova Z, Hickey M, Vaarmann A, Mandel M, Zeb A, Choubey V, Kuum M, Safiulina D, Vasar E, Veksler V, Kaasik A (2016) Role of mitochondrial dynamics in neuronal development: mechanism for wolfram syndrome. *PLoS Biol* 14: e1002511

Chan N, Salazar A, Pham A, Sweredoski M, Kolawa N, Graham R, Hess S, Chan D (2011) Broad activation of the ubiquitin–proteasome system by Parkin is critical for mitophagy. *Hum Mol Genet* 20: 1726 – 1737

Chen L, Liu C, Gao J, Xie Z, Chan L, Keating D, Yang Y, Sun J, Zhou F, Wei Y, Men X, Yang S (2017) Inhibition of Miro1 disturbs mitophagy and pancreatic β-cell function interfering insulin release via IRS-Akt-Foxo1 in diabetes. *Oncotarget* 8: 90693 – 90705

Cherra S, Steer E, Gusdon A, Kiselyov K, Chu C (2013) Mutant LRRK2 elicits calcium imbalance and depletion of dendritic mitochondria in neurons. *Am J Pathol* 182: 474 – 484

Choubey V, Safiulina D, Vaarmann A, Cagalinec M, Wareski P, Kuum M, Zharkovsky A, Kaasik A (2011) Mutant A53T α-synuclein induces neuronal death by increasing mitochondrial autophagy. *J Biol Chem* 286: 10814 – 10824

Choubey V, Cagalinec M, Liiv J, Safiulina D, Hickey M, Kuum M, Liiv M, Anwar T, Eskelinen E, Kaasik A (2014) BECN1 is involved in the initiation of mitophagy. *Autophagy* 10: 1105 – 1119

East D, Campanella M (2013) Ca^{2+} in quality control. *Autophagy* 9: 1710 – 1719

Fransson Å, Ruusala A, Aspenström P (2003) Atypical Rho GTPases have roles in mitochondrial homeostasis and apoptosis. *J Biol Chem* 278: 6495 – 6502

Frederick R, McCaffery J, Cunningham K, Okamoto K, Shaw J (2004) Yeast Miro GTPase, Gem1p, regulates mitochondrial morphology via a novel pathway. *J Cell Biol* 167: 87 – 98

Geisler S, Holmström K, Skujat D, Fiesel F, Rothfuss O, Kahle P, Springer W (2010) PINK1/Parkin-mediated mitophagy is dependent on VDAC1 and p62/SQSTM1. *Nat Cell Biol* 12: 119 – 131

Gómez-Sánchez R, Gegg M, Bravo-San Pedro J, Niso-Santano M, Alvarez-Erviti L, Pizarro-Estrella E, Gutiérrez-Martín Y, Alvarez-Barrientos A, Fuentes J, González-Polo R, Schapira A (2014) Mitochondrial impairment increases FL-PINK1 levels by calcium-dependent gene expression. *Neurobiol Dis* 62: 426 – 440

Guo X, Macleod G, Wellington A, Hu F, Panchumarthi S, Schoenfield M, Marin L, Charlton M, Atwood H, Zinsmaier K (2005) The GTPase dMiro is required for axonal transport of mitochondria to *Drosophila* synapses. *Neuron* 47: 379 – 393

Hattori N, Matsumine H, Asakawa S, Kitada T, Yoshino H, Elibol B, Brookes AJ, Yamamura Y, Kobayashi T, Wang M, Yoritaka A, Minoshima S, Shimizu N, Mizuno Y (1998) Point mutations (Thr240Arg and Ala311Stop) in the Parkin gene. *Biochem Biophys Res Commun* 249: 754 – 758

Kazlauskaite A, Kelly V, Johnson C, Baillie C, Hastie C, Peggie M, Macartney T, Woodroof H, Alessi D, Pedrioli P, Muqit M (2014a) Phosphorylation of Parkin at Serine65 is essential for activation: elaboration of a Miro1 substrate-based assay of Parkin E3 ligase activity. *Open Biol* 4: 130213 – 130213

Kazlauskaite A, Kondapalli C, Gourlay R, Campbell D, Ritorto M, Hofmann K, Alessi D, Knebel A, Trost M, Muqit M (2014b) Parkin is activated by PINK1-dependent phosphorylation of ubiquitin at Ser65. *Biochem J* 460: 127 – 141

Kazlauskaite A, Martinez-Torres R, Wilkie S, Kumar A, Peltier J, Gonzalez A, Johnson C, Zhang J, Hope A, Peggie M, Trost M, van Aalten D, Alessi D, Prescott A, Knebel A, Walden H, Muqit M (2015) Binding to serine 65-phosphorylated ubiquitin primes Parkin for optimal PINK1-dependent phosphorylation and activation. *EMBO Rep* 16: 939 – 954

Klosowiak J, Focia P, Chakravarthy S, Landahl E, Freymann D, Rice S (2013) Structural coupling of the EF hand and C-terminal GTPase domains in the mitochondrial protein Miro. *EMBO Rep* 14: 968 – 974

Klosowiak J, Park S, Smith K, French M, Focia P, Freymann D, Rice S (2016) Structural insights into Parkin substrate lysine targeting from minimal Miro substrates. *Sci Rep* 6: 33019

Koyano F, Okatsu K, Kosako H, Tamura Y, Go E, Kimura M, Kimura Y, Tsuchiya H, Yoshihara H, Hirokawa T, Endo T, Fon E, Trempe J, Saeki Y, Tanaka K,

Matsuda N (2014) Ubiquitin is phosphorylated by PINK1 to activate parkin. *Nature* 510: 162 – 166

Lazarou M, Narendra D, Jin S, Tekle E, Banerjee S, Youle R (2013) PINK1 drives Parkin self-association and HECT-like E3 activity upstream of mitochondrial binding. *J Cell Biol* 200: 163 – 172

Lazarou M, Sliter D, Kane L, Sarraf S, Wang C, Burman J, Sideris D, Fogel A, Youle R (2015) The ubiquitin kinase PINK1 recruits autophagy receptors to induce mitophagy. *Nature* 524: 309 – 314

Liu S, Sawada T, Lee S, Yu W, Silverio G, Alapatt P, Millan I, Shen A, Saxton W, Kanao T, Takahashi R, Hattori N, Imai Y, Lu B (2012) Parkinson's disease-associated kinase PINK1 regulates Miro protein level and axonal transport of mitochondria. *PLoS Genet* 8: e1002537

López-Doménech G, Higgs N, Vaccaro V, Roš H, Arancibia-Cárcamo I, MacAskill A, Kittler J (2016) Loss of dendritic complexity precedes neurodegeneration in a mouse model with disrupted mitochondrial distribution in mature dendrites. *Cell Rep* 17: 317 – 327

MacAskill A, Rinholm J, Twelvetrees A, Arancibia-Carcamo I, Muir J, Fransson A, Aspenstrom P, Attwell D, Kittler J (2009) Miro1 is a calcium sensor for glutamate receptor-dependent localization of mitochondria at synapses. *Neuron* 61: 541 – 555

MacVicar T, Mannack L, Lees R, Lane J (2015) Targeted siRNA screens identify ER-to-mitochondrial calcium exchange in autophagy and mitophagy responses in RPE1 cells. *Int J Mol Sci* 16: 13356 – 13380

Martinez A, Lectez B, Ramirez J, Popp O, Sutherland J, Urbé S, Dittmar G, Clague M, Mayor U (2017) Quantitative proteomic analysis of Parkin substrates in *Drosophila* neurons. *Mol Neurodegener* 12: 29

Nguyen T, Oh S, Weaver D, Lewandowska A, Maxfield D, Schuler M, Smith N, Macfarlane J, Saunders G, Palmer C, Debattisti V, Koshiba T, Pulst S, Feldman E, Hajnoczky G, Shaw J (2014) Loss of Miro1-directed mitochondrial movement results in a novel murine model for neuron disease. *Proc Natl Acad Sci USA* 111: E3631 – E3640

Okatsu K, Koyano F, Kimura M, Kosako H, Saeki Y, Tanaka K, Matsuda N (2015) Phosphorylated ubiquitin chain is the genuine Parkin receptor. *J Cell Biol* 209: 111 – 128

Ordureau A, Sarraf S, Duda D, Heo J, Jedrychowski M, Sviderskiy V, Olszewski J, Koerber J, Xie T, Beausoleil S, Wells J, Gygi S, Schulman B, Harper J (2014) Quantitative proteomics reveal a feedforward mechanism for mitochondrial Parkin translocation and ubiquitin chain synthesis. *Mol Cell* 56: 360 – 375

Ordureau A, Heo J, Duda D, Paulo J, Olszewski J, Yanishevski D, Rinehart J, Schulman B, Harper J (2015) Defining roles of PARKIN and ubiquitin phosphorylation by PINK1 in mitochondrial quality control using a ubiquitin replacement strategy. *Proc Natl Acad Sci USA* 112: 6637 – 6642

Park S, Foote P, Krist D, Rice S, Statsyuk A (2017) UbMES and UbFluor: novel probes for ring-between-ring (RBR) E3 ubiquitin ligase PARKIN. *J Biol Chem* 292: 16539 – 16553

Rimessi A, Bonora M, Marchi S, Patergnani S, Marobbio C, Lasorsa F, Pinton P (2013) Perturbed mitochondrial Ca2+signals as causes or consequences of mitophagy induction. *Autophagy* 9: 1677 – 1686

Saotome M, Safiulina D, Szabadkai G, Das S, Fransson A, Aspenstrom P, Rizzuto R, Hajnoczky G (2008) Bidirectional Ca2+-dependent control of mitochondrial dynamics by the Miro GTPase. *Proc Natl Acad Sci USA* 105: 20728 – 20733

Sarraf S, Raman M, Guarani-Pereira V, Sowa M, Huttlin E, Gygi S, Harper J (2013) Landscape of the PARKIN-dependent ubiquitylome in response to mitochondrial depolarization. *Nature* 496: 372 – 376

Schinder AF, Olson EC, Spitzer NC, Montal M (1996) Mitochondrial dysfunction is a primary event in glutamate neurotoxicity. *J Neurosci* 16: 6125 – 6133

Shiba-Fukushima K, Arano T, Matsumoto G, Inoshita T, Yoshida S, Ishihama Y, Ryu K, Nukina N, Hattori N, Imai Y (2014) Phosphorylation of mitochondrial polyubiquitin by PINK1 promotes Parkin mitochondrial tethering. *PLoS Genet* 10: e1004861

Sun Y, Vashisht A, Tchieu J, Wohlschlegel J, Dreier L (2012) Voltage-dependent anion channels (VDACs) recruit parkin to defective mitochondria to promote mitochondrial autophagy. *J Biol Chem* 287: 40652 – 40660

Tang M, Vranas M, Krahn A, Pundlik S, Trempe J, Fon E (2017) Structure-guided mutagenesis reveals a hierarchical mechanism of Parkin activation. *Nat Commun* 8: 14697

Vaarmann A, Mandel M, Zeb A, Wareski P, Liiv J, Kuum M, Antsov E, Liiv M, Cagalinec M, Choubey V, Kaasik A (2016) Mitochondrial biogenesis is required for axonal growth. *Development* 143: 1981 – 1992

Van Laar V, Roy N, Liu A, Rajprohat S, Arnold B, Dukes A, Holbein C, Berman S (2015) Glutamate excitotoxicity in neurons triggers mitochondrial and endoplasmic reticulum accumulation of Parkin, and in the presence of N-acetyl cysteine, mitophagy. *Neurobiol Dis* 74: 180 – 193

Wang X, Schwarz T (2009) The mechanism of Ca^{2+}-dependent regulation of kinesin-mediated mitochondrial motility. *Cell* 136: 163 – 174

Wang X, Winter D, Ashrafi G, Schlehe J, Wong Y, Selkoe D, Rice S, Steen J, LaVoie M, Schwarz T (2011) PINK1 and Parkin target Miro for phosphorylation and degradation to arrest mitochondrial motility. *Cell* 147: 893 – 906

Weihofen A, Thomas K, Ostaszewski B, Cookson M, Selkoe D (2009) Pink1 forms a multiprotein complex with Miro and milton, linking Pink1 function to mitochondrial trafficking. *Biochemistry* 48: 2045 – 2052

White RJ, Reynolds IJ (1996) Mitochondrial depolarization in glutamate-stimulated neurons: an early signal specific to excitotoxin exposure. *J Neurosci* 16: 5688 – 5697